

# Heavy Quark Radiative Energy Loss in QCD Matter

Magdalena Djordjevic and Miklos Gyulassy

*Dept. Physics, Columbia University, 538 W 120-th Street,  
New York, NY 10027, USA*

February 8, 2008

## Abstract

Heavy quark medium induced radiative energy loss is derived to all orders in opacity,  $(L/\lambda_g)^n$ . The analytic expression generalizes the GLV opacity expansion for massless quanta to heavy quarks with mass  $M$  in a QCD plasma with a gluon dispersion characterized by an asymptotic plasmon mass,  $m_g = gT/\sqrt{2}$ . Remarkably, we find that the general result is obtained by simply shifting all frequencies in the GLV series by  $(m_g^2 + x^2 M^2)/(2xE)$ . Numerical evaluation of the first order in opacity energy loss shows that both charm and bottom energy losses are much closer to the incoherent radiation limit than light partons in nuclear collisions at both RHIC and LHC energies. However, the radiation lengths of heavy quarks remain large compared to nuclear dimensions and hence high  $p_T$  heavy quark production is volume rather than surface dominated.

## 1 Introduction

The discovery [1]-[8] of a factor of  $4 \sim 5$  suppression of high  $p_\perp \sim 5 - 10$  GeV hadrons produced in central  $Au + Au$  at the Relativistic Heavy Ion Collider (RHIC) has been interpreted as evidence for jet quenching of light quark and gluon jets [9]-[19]. Jet quenching was predicted [20] to occur due to radiative energy loss of high energy partons that propagate through ultra-dense QCD matter. The observed quenching pattern is interesting not only as a test of QCD multiple scattering theory but also because it provides a novel tomographic tool that can be used to map the evolution of the quark gluon plasma (QGP) produced in ultra-relativistic nuclear collisions. Medium induced radiation arises from higher twist final state interactions and depends on the integrated optical thickness or gluonic opacity  $L/\lambda_g$  of the QCD medium. At high  $p_T$  it dominates over the energy loss due to elastic scattering [21].

Recent data from RHIC  $D + Au$  reactions [22]-[25], on the other hand, show the absence of jet quenching in such light ion beam reactions. These data are in accord with predictions based on jet tomography in Refs. [10, 11, 12] because in light ion interactions no extended dense QCD medium is produced in the final state. This important  $D + Au$  control experiment therefore strengthens the interpretation of the observed high  $p_T$  quenching pattern in central  $Au + Au$  as due to final state energy loss of jets produced in dense QGP matter.

The first estimates for heavy quark energy loss [26]-[28] proposed that similar quenching may occur for charm jets as for light partons. However, in ref. [29] it was pointed out that the heavy quark mass leads to a kinematical “dead cone” effect for  $\theta < M/E$  that reduces significantly the induced radiative energy loss of heavy quarks. Numerical estimates indicated that the quenching of charm quarks may be about a half that of light quarks. Experimentally, the first PHENIX data [30] on “prompt” single electron production in  $Au + Au$  collisions at  $\sqrt{s} = 130$  AGeV provided a first rough look at heavy quark transverse momentum distributions at RHIC. Remarkably, no indication for a QCD medium effect was found within the admittedly large experimental errors (see also ref. [31]). However, in the near future, data with much higher statistics and wider  $p_T$  range will become accessible.

We concentrate in this paper on the theory of heavy quark energy loss, extending our previous works I [32] and II [33]. Their quenching pattern and correlations should provide independent complementary tests of QGP production. In addition, heavy quark observables can be used to test different approximations in the emerging theories of heavy quark radiative energy loss QCD [26]-[29], [32]-[34]. The main new feature that heavy quark probes introduce is a controlled reduction of the radiated gluon formation times due to finite mass kinematic effects. As the mass increases, the increase of phase shifts leads to a reduction [32] of destructive Landau-Pomeanchuk-Migdal (LPM) interference effects that were found to be so important for light quark or gluon jet energy loss [9]-[19]. In addition, the kinematic reduction of propagator amplitudes leads to an overall decrease of the magnitude of heavy energy loss relative to light jet energy loss even in the incoherent Gunion-Bertsch [35] (GB) limit, as we demonstrate quantitatively below. Therefore, the predictable high  $p_T$  open charm and open bottom observables at RHIC and LHC will provide interesting new control tests of QCD dynamics in nuclear collisions.

The main goal of this paper is (1) to generalize the GLV opacity series [16] to include massive quark kinematic effects and (2) to take into account the Ter-Mikayelian plasmon effects for gluons as described in Ref. [33]. The competition between these two medium effects was first discussed in our paper I [32]. We showed that the apparent null effect observed for heavy quarks via single electrons could in part be due to a reduction of the leading  $O(\chi^0)$  order radiation *associated* with the initial hard production process. In this sense, there are two opposing medium effects: (1) at  $O(\chi^0)$ , the Ter-Mikayelian plasmon dispersion effect that reduces the *associated* hard radiation energy loss [33] and (2) at  $O(\chi^{n \geq 1})$ , the *induced* radiative energy loss that increases the total radiative energy loss albeit with a reduced efficiency due to the dead cone effect [29]. The detailed derivation of the QCD Ter-Mikayelian effect was presented in paper II [33]. An important conclusion from II, which we rely on in the derivation below, was that the effects due to the plasmon dispersion relation can be well approximated for high  $p_T$  jets ignoring the longitudinal modes and applying the asymptotic (short wavelength transverse) plasmon mass. That asymptotic mass,  $m_g = \mu/\sqrt{2}$  is somewhat larger than the long wavelength plasmon mass  $\mu/\sqrt{3}$ , where  $\mu \approx gT$  GeV is chromoelectric Debye screening mass.

We concentrate here as in [16] on the case of high  $p_T$  eikonal jets produced inside a finite evolving QGP at some initial point  $(t_0, z_0, \mathbf{x}_0)$ . This is in contrast to the Gunion-Bertsch problem [35] with  $t_0 = -\infty$ , where the jet is prepared as a beam in the remote past. We model the interactions in the QGP as in [16, 17] via random color screened potentials

$$V_n = V(q_n)e^{iq_n x_n} = 2\pi\delta(q^0)v(\vec{\mathbf{q}}_n)e^{-i\vec{\mathbf{q}}_n \cdot \vec{\mathbf{x}}_n} T_{a_n}(R) \otimes T_{a_n}(n) , \quad (1)$$

where  $\vec{\mathbf{x}}_n$  is the location of the  $n^{\text{th}}$  scattering center and  $v(\vec{\mathbf{q}}_n) \equiv 4\pi\alpha_s/(\vec{\mathbf{q}}_n^2 + \mu^2)$ . The elastic cross section between the jet and target partons in the GW model is

$$\frac{d\sigma_{el}(R, T)}{d^2\mathbf{q}} = \frac{C_R C_2(T)}{d_A} \frac{|v(\mathbf{q})|^2}{(2\pi)^2} . \quad (2)$$

For consistency with GLV [16], we use the same notation throughout. Transverse 2D vectors are denoted as bold  $\mathbf{p}$ , 3D vectors as vectors  $\vec{\mathbf{p}} = (p_z, \mathbf{p})$ , and four vectors by  $p = (p^0, \vec{\mathbf{p}}) = [p^0 + p^z, p^0 - p^z, \mathbf{p}]$ . The color exchange bookkeeping with the target parton  $n$  is handled by an appropriate  $SU(N_c)$  generator [16],  $T_a(n)$ , in the  $d_n$  dimensional representation of the target ( $\text{Tr} T_a(n) = 0$  and  $\text{Tr}(T_a(i)T_b(j)) = \delta_{ij}\delta_{ab}C_2(i)d_i/d_A$ ). We assume that all target partons are in the same  $d_T$  dimensional representation with Casimir  $C_2(T)$ .) We denote the generators in the  $d_R$  dimensional representation corresponding to the jet by  $a \equiv t_a$  with  $aa = C_R \mathbf{1}$ . For heavy quarks in  $SU(3)$ ,  $C_R = 4/3$  while  $C_A = 3$ . The elastic cross section of target parton  $i$  with the jet is therefore proportional to the product of Casimirs,  $C_R C_2(T)$ . As in [16], the analytic results derived below with the reaction operator approach do not depend on the actual form of  $v$ , but the Yukawa form will be used for convenience in numerical estimates.

The sections are organized as follows: In section 2, we review the zeroth order in opacity but in medium *associated* radiation for a massive quark jets. At zeroth order only the hard initial vertex acts as a source

for gluon radiation, but in a medium the dynamical gluon mass,  $\sqrt{\omega_{pl}^2(k) - k^2} \approx m_g$  is taken into account [33]. In section 3, the first order in opacity heavy quark energy loss is computed. We improve Eq. (2) in paper I [32] ( see Eq. (12) below) by incorporating more carefully the kinematic constraints so that the GLV massless  $M \rightarrow 0$  limit can be recovered. The detailed diagrammatic computations are recorded in Appendices A-G closely following the derivation in GLV [16] but pointing out the different phases and residues that arise when  $M$  and  $m_g$  are not zero. Section 4, presents the generalization of GLV to all orders in opacity for finite masses. Our main result (Eq.(17)), which follows from the reaction operator method using the results from the appendices, is that the analytic structure of the small- $x$  induced radiation distribution in the heavy quark case is identical to that of the massless case but with a single universal energy shift  $\Delta\omega = (m_g^2 + x^2 M^2)/(2xE)$ . The energy shift is independent of the momentum transfers  $\mathbf{q}_i$  and the plasmon transverse momentum  $\mathbf{k}$ . In section 5 we give numerical estimates for the the first order energy loss of charm and bottom quarks comparing RHIC and LHC conditions. We show quantitatively how close our (partially coherent) numerical results are to the incoherent limit. Conclusions are presented in section 6.

## 2 The one gluon associated radiation

In order to compute the associated radiative energy loss when the hard process is embedded in a dielectric medium, we need to compute the squared amplitude of Feynman diagram,  $M_{rad}^0$ , which represents the source  $J$  that produces an off-shell jet with momentum  $p'$  and subsequently radiates a gluon obeying the dispersion relation,  $\omega(k)$ , of the medium with momentum  $k$ . The jet emerges with momentum  $p$  and mass  $M$ . Since our focus is on heavy quarks, we neglect the thermal shifts of the heavy quark mass here. As noted before, the detailed computation of the associated energy loss was done in [33], where it was shown that gluons in the medium can be approximated as massive transverse plasmons with mass  $m_g \approx m_\infty = \mu/\sqrt{2}$ .

If we assume that  $p_z$  and  $k_z$  are large enough, such that  $M^2/p_z^2 \ll 1$  and  $m_g^2/k_z^2 \ll 1$  are satisfied, then we can write  $p$ ,  $k$ , and the transverse polarization  $\epsilon$  in terms of light cone components:

$$k = [xE^+, k^-, \mathbf{k}] , \epsilon(k) = [0, 2\frac{\epsilon \cdot \mathbf{k}}{xE^+}, \epsilon] , \mathbf{p} = [(1-x)\mathbf{E}^+, \mathbf{p}^-, \mathbf{p}] . \quad (3)$$

Soft radiation is defined as  $x \ll 1$  so that, for example,  $p^+ \gg k^+$  and  $p^- = (\mathbf{p}^2 + M^2)/(1-x)E^+ \ll k^- = (\mathbf{k}^2 + m_g^2)/xE^+$ . Here,  $M$  is the mass of the quark, and  $m_g$  is the mass of the glue of energy  $\omega \approx xE^+/2$ . We also adopt the same shorthand notation as in [16] for energy differences:

$$\omega_0 = \frac{\mathbf{k}^2}{2\omega} , \omega_i = \frac{(\mathbf{k} - \mathbf{q}_i)^2}{2\omega} , \omega_{(ij)} = \frac{(\mathbf{k} - \mathbf{q}_i - \mathbf{q}_j)^2}{2\omega} . \quad (4)$$

In the soft eikonal kinematics that we consider

$$E^+ \gg k^+ \gg \omega_{(i\dots j)} + \frac{m_g^2}{2\omega} \gg \frac{(\mathbf{p} + \mathbf{k})^2 + M^2}{E^+} . \quad (5)$$

The hard jet radiation amplitude to emit a transverse plasmon with momentum, polarization, and color  $(k, \epsilon, c)$  without final state interactions is

$$\begin{aligned} M_{rad}^0 &= iJ(p+k)e^{i(p+k)x_0}(ig_s)(2p+k)_\mu \epsilon^\mu(k) i\Delta_M(p+k)c \\ &\approx J(p)e^{ipx_0}(-2ig_s)\frac{\epsilon \cdot \mathbf{k}}{k^2 + m_g^2 + M^2x^2} e^{i\omega_0 z_0} c , \end{aligned} \quad (6)$$

where  $x_0(0, z_0, \mathbf{0})$  is the jet production point inside the plasma. We assume, as in [16], that  $J$  varies slowly with  $p$ , and neglect high  $x$  spin effects. Eq.(6) represents the mass corrections to the Eg.(35) in [16]. In soft radiation approximation the spectrum can be extracted as

$$|M_{rad}^0|^2 \frac{d^3 \vec{\mathbf{p}}}{2E(2\pi)^3} \frac{d^3 \vec{\mathbf{k}}}{2\omega(2\pi)^3} \approx d^3 N_J d^3 N_g^{(0)} , \quad (7)$$

where (with  $d_R = 3$  dimensional representation quarks)

$$d^3 N_J = d_R |J(p)|^2 \frac{d^3 \vec{\mathbf{p}}}{(2\pi)^3 2p^0} . \quad (8)$$

Eqs. (7, 8) lead to the finite mass generalization of the small  $x$  invariant DGLAP radiation spectrum

$$\omega \frac{dN_g^{(0)}}{d^3 \vec{\mathbf{k}}} \approx x \frac{dN_g^{(0)}}{dx d^2 \vec{k}_\perp} \approx \frac{C_R \alpha_s}{\pi^2} \frac{\mathbf{k}^2}{(\mathbf{k}^2 + m_g^2 + x^2 M^2)^2} . \quad (9)$$

Eq. (9) clearly shows the depletion of radiation in the ‘‘dead cone’’ [29] at angles

$$\theta < \theta_c = \sqrt{m_g^2 + x^2 M^2} / (xE)$$

generalized to take into account also the Ter-Mikayelian dielectric dispersion in a QGP.

### 3 First order radiative energy loss

The first order in opacity energy loss can be computed from formula:

$$d^3 N_g^{(1)} d^3 N_J = \left( \frac{1}{d_T} \text{Tr} \langle |M_1|^2 \rangle + \frac{2}{d_T} \text{ReTr} \langle M_0^* M_2 \rangle \right) \frac{d^3 \vec{\mathbf{p}}}{(2\pi)^3 2p^0} \frac{d^3 \vec{\mathbf{k}}}{(2\pi)^3 2\omega} , \quad (10)$$

where  $d^3 N_J$  is given by Eq. (8) and  $d_T$  is the dimension of the target color representation (= 8 for a pure gluon plasma).  $M_1$  is sum of all diagrams with one scattering center and  $M_2$  is sum of all diagrams with two scattering centers in the contact limit. We compute those diagrams using the same assumptions as in [16], as reviewed in Appendix A. The detailed evaluation of the amplitudes is presented in Appendices B-F. The results are combined in appendix G, to give the small  $x$  differential energy loss

$$\begin{aligned} \frac{dE_{ind}^{(1)}}{dx} &= \frac{C_R \alpha_S}{\pi} \frac{L}{\lambda} E \int \frac{d\mathbf{k}^2}{\mathbf{k}^2 + m_g^2 + M^2 x^2} \int \frac{d^2 \mathbf{q}_1}{\pi} \frac{\mu^2}{(\mathbf{q}_1^2 + \mu^2)^2} \times \\ &\times 2 \frac{\mathbf{k} \cdot \mathbf{q}_1 (\mathbf{k} - \mathbf{q}_1)^2 + (m_g^2 + M^2 x^2) \mathbf{q}_1 \cdot (\mathbf{q}_1 - \mathbf{k})}{\left(\frac{4Ex}{L}\right)^2 + ((\mathbf{k} - \mathbf{q}_1)^2 + M^2 x^2 + m_g^2)^2} , \end{aligned} \quad (11)$$

where  $|\mathbf{q}_1|$  is the magnitude of the transverse momentum transfer between a target parton and a jet,  $|\mathbf{k}|$  is the magnitude of the transverse momentum of the radiated gluon, and  $\lambda_g$  is the mean free path of the gluon. The simple analytic form of the destructive interference factor involving  $(4Ex/L)^2$  arises for an assumed exponential distribution  $\exp(-\Delta z/L)/L$  of the distance between the jet production and target rescattering center. Note that in the massless limit,  $M = m_g = 0$ , Eq. (11) reduces to Eq. (125) in [16].

Numerical evaluation of Eq.11 shows that to a good approximation we can ignore the finite kinematic bounds on  $|\mathbf{q}_1| < \sqrt{6ET}$  for  $E > 10$  GeV charm jets. With this simplification, we can substitute  $\mathbf{q} \rightarrow \mathbf{q}_1 - \mathbf{k}$  and integrate over the azimuthal angle to arrive at

$$\Delta E_{ind}^{(1)} = \frac{C_F \alpha_S L}{\pi \lambda_g} \int_0^1 dx E \int_0^\infty \frac{2\mathbf{q}^2 \mu^2 d\mathbf{q}^2}{\left(\frac{4Ex}{L}\right)^2 + (\mathbf{q}^2 + M^2 x^2 + m_g^2)^2} \int \frac{d\mathbf{k}^2 \theta(xE - |\mathbf{k}|)}{((|\mathbf{k}| - |\mathbf{q}|)^2 + \mu^2)^{3/2} ( (|\mathbf{k}| + |\mathbf{q}|)^2 + \mu^2)^{3/2}} \left\{ \mu^2 + (\mathbf{k}^2 - \mathbf{q}^2) \frac{\mathbf{k}^2 - M^2 x^2 - m_g^2}{\mathbf{k}^2 + M^2 x^2 + m_g^2} \right\}, \quad (12)$$

If we further neglect the finite kinematic boundaries on the gluon transverse momentum,  $|\mathbf{k}| < xE$ , then in the massless  $M = m_g = 0$  limit, we recover the approximate asymptotic Eq. (127) of [16]. The  $\mathbf{k}^2$  integral in Eq. (12) can be performed analytically if  $\alpha_S$  does not run, but the cumbersome result is not instructive.

We note that Eq. (12) differs from the Eq. (2) in [33]. The  $\Delta E_{ind}^{(1)}$  in [33] was obtained by assuming that energy of the glue is much larger than momentum transfer  $\mathbf{q}_1$ , i.e  $xE \pm |\mathbf{q}_1| \approx xE$ . Eq. (12) avoids this approximation by incorporating exact kinematics at the price of a more complicated expression. Numerically, this improvement however, does not change significantly the estimated charm energy loss presented in [33] as shown in section 5. However, theoretically, Eq. (12) is preferred since the  $M \rightarrow 0$  limit is only correctly recovered when exact kinematics are enforced.

The main qualitative effect of increasing  $M$  is to reduce the relevance of the inverse formation time factor  $(4Ex/L)^2$  in the denominator of the integrand. Formally, by setting this factor to zero recovers the incoherent limit of induced radiation. This corresponds to the QCD analog of the QED Bethe-Heitler limit with  $\Delta E_{GB} \propto \alpha_s EL/\lambda_g$  modulo a logarithmic factor. In QCD this includes the isolated scattering Gunion-Bertsch (GB) radiation as well as elastic scattering of the associated radiation from zeroth order in opacity as we discuss in the following section.

The incoherent, short formation time limit, generalized here to include the plasmon asymptotic mass, is given by

$$\frac{\Delta E_{in}}{E} = \frac{C_F \alpha_S L}{\pi \lambda_g} \int_0^1 dx \int \frac{2\mathbf{q}^2 \mu^2 d\mathbf{q}^2}{(\mathbf{q}^2 + M^2 x^2 + m_g^2)^2} \int \frac{d\mathbf{k}^2 \theta(xE - |\mathbf{k}|)}{((|\mathbf{k}| - |\mathbf{q}|)^2 + \mu^2)^{3/2} ( (|\mathbf{k}| + |\mathbf{q}|)^2 + \mu^2)^{3/2}} \left\{ \mu^2 + (\mathbf{k}^2 - \mathbf{q}^2) \frac{\mathbf{k}^2 - M^2 x^2 - m_g^2}{\mathbf{k}^2 + M^2 x^2 + m_g^2} \right\}, \quad (13)$$

Since we found in Ref. [32], and show in more detail in section 5 that the heavy quark energy loss is close to the incoherent limit, it is also useful to define the effective gluon radiation length,  $L_{rad}$ , via

$$\frac{d\Delta E}{dL} \equiv \frac{E}{L_{rad}(M, m_g, E, L)}. \quad (14)$$

This length is of relevance to answer the question whether the jets observed in a given kinematic window are dominated by surface or volume emission.

## 4 Higher orders in opacity energy loss

### 4.1 Heavy quark generalization of GLV to all orders

From the results of the calculations reported in the appendices, we find that the finite masses modify the effective radiation amplitudes and phase factors in a remarkably simple and universal way. The phase factors in

the massless case studied in GLV [16] modulate the amplitudes by factors such as  $Exp(i \sum_m \omega_{(m \dots n)} \Delta z_m)$ . The energy differences  $\omega_{(m \dots n)}$  from Eq.(4) are inverse formation times and  $\Delta z_m$  are distances between scattering centers. With finite  $M$  and  $m_g$  these energy differences are found from Eqs. (41, 45, 51, 60, 66, 67, 72) to be simply shifted by a  $q_i$  independent term,

$$\omega_{(m, \dots, n)} = \frac{(\mathbf{k} - \mathbf{q}_m - \dots - \mathbf{q}_n)^2}{2xE} \rightarrow \Omega_{(m, \dots, n)} \equiv \omega_{(m, \dots, n)} + \frac{m_g^2 + M^2 x^2}{2xE} \quad (15)$$

In addition, the kinematic current amplitudes appearing in those equations are simply modified versions of the Hard, Gluon-Bertsch and Cascade terms in GLV, which for finite masses are now

$$\begin{aligned} \tilde{\mathbf{H}} &= \frac{\mathbf{k}}{\mathbf{k}^2 + m_g^2 + M^2 x^2}, & \tilde{\mathbf{C}}_{(i_1 i_2 \dots i_m)} &= \frac{(\mathbf{k} - \mathbf{q}_{i_1} - \mathbf{q}_{i_2} - \dots - \mathbf{q}_{i_m})}{(\mathbf{k} - \mathbf{q}_{i_1} - \mathbf{q}_{i_2} - \dots - \mathbf{q}_{i_m})^2 + m_g^2 + M^2 x^2}, \\ \tilde{\mathbf{B}}_i &= \tilde{\mathbf{H}} - \tilde{\mathbf{C}}_i, & \tilde{\mathbf{B}}_{(i_1 i_2 \dots i_m)(j_1 j_2 \dots j_n)} &= \tilde{\mathbf{C}}_{(i_1 i_2 \dots j_m)} - \tilde{\mathbf{C}}_{(j_1 j_2 \dots j_n)}. \end{aligned} \quad (16)$$

In summary, the computations in Appendices B-F show that the diagrams for the finite masses case can be obtained from corresponding massless equations in [16], by simply replacing the terms from Eqs. (58, 106) in [16] by the modified terms defined in Eqs. (16, 15).

Therefore, the recursive GLV reaction operator formalism carries over to the massive case with the simple replacements above. The complete arbitrary order in opacity induced radiation distribution can be obtained by generalizing Eq.(113) of GLV as follows:

$$\begin{aligned} x \frac{dN^{(n)}}{dx d^2 \mathbf{k}} &= \frac{C_R \alpha_s}{\pi^2} \frac{1}{n!} \int \prod_{i=1}^n \left( d^2 \mathbf{q}_i \frac{L}{\lambda_g(i)} [\bar{v}_i^2(\mathbf{q}_i) - \delta^2(\mathbf{q}_i)] \right) \times \\ &\times \left( -2 \tilde{\mathbf{C}}_{(1, \dots, n)} \cdot \sum_{m=1}^n \tilde{\mathbf{B}}_{(m+1, \dots, n)(m, \dots, n)} \left[ \cos \left( \sum_{k=2}^m \Omega_{(k, \dots, n)} \Delta z_k \right) - \cos \left( \sum_{k=1}^m \Omega_{(k, \dots, n)} \Delta z_k \right) \right] \right), \end{aligned} \quad (17)$$

where  $\sum_2^1 \equiv 0$  is understood and  $|\bar{v}_i(\mathbf{q}_i)|^2$  is defined as the normalized distribution of momentum transfers from  $i^{\text{th}}$  scattering center [16]. For the Yukawa screened interactions (Eq. (2)), the differential gluon cross section in the local density approximation is

$$\sigma(z_i, \mathbf{q}_i) \equiv \sigma_{el}(z_i) |\bar{v}_i(\mathbf{q}_i)|^2 = \frac{d^2 \sigma_{el}(z_i)}{d^2 \mathbf{q}_i} = \frac{\sigma_{el}(z_i)}{\pi} \frac{\mu(z_i)^2}{(\mathbf{q}^2 + \mu(z_i)^2)^2}, \quad (18)$$

where  $\mu(z_i)$  is the local Debye mass that may vary if the system expands.

Note that, as in [16] the Eq. (17) is not restricted to uncorrelated geometries. Also it allows the inclusion of finite kinematic boundaries on the  $\mathbf{q}_i$  as well as different functional forms of the gluon elastic cross sections along the eikonal path. The  $n^{\text{th}}$  order in opacity energy loss spectrum can be obtained from Eq. (17) via

$$\frac{dE^{(n)}}{dx} = \int d^2 \mathbf{k} \frac{dN^{(n)}}{dx d^2 \mathbf{k}} xE \quad (19)$$

From the Eqs. (17, 19) we can obtain the first order in opacity energy loss by setting  $n = 1$ . The result obtained after averaging over  $\exp(-\Delta z_1/L)/L$  is the same as Eq. (84) in Appendix G, which leads to Eq. (12) computed in previous section.

In order to make the averaging over the target coordinates more explicit, assume an uncorrelated geometry and let  $\rho(z) \equiv \rho(z, \tau = z)$  denote the target density along the path of the jet. For Bjorken expansion  $\rho(z) = \theta(R - z)\rho_0\tau_0/z$  for example. In the local density approximation, the screening mass,  $\mu(z)$ , may also depend on the proper time ( $\tau = z$ ). Then  $\sigma_{el}(z)$  and  $|\bar{v}(z, \mathbf{q})|^2$  may vary along the jet path as well. The average over over the target centers can be made explicit by replacing the opacity factor in (17) by

$$\frac{1}{n!} \int \prod_{i=1}^n \left( d^2 \mathbf{q}_i \frac{L}{\lambda_g(i)} [\bar{v}_i^2(\mathbf{q}_i) - \delta^2(\mathbf{q}_i)] \right) \rightarrow \int_0^\infty dz_1 \rho(z_1) \cdots \int_{z_{n-1}}^\infty dz_n \rho(z_n) \times \int \prod_{i=1}^n (d^2 \mathbf{q}_i [\sigma(z, \mathbf{q}_i) - \sigma_{el}(z)\delta^2(\mathbf{q}_i)]) \quad (20)$$

## 4.2 The Incoherent, Short Formation Time Limit

The incoherent limit of Eq.(17) is obtained formally by taking the large  $\Omega_{(k, \dots, n)} \Delta z_k \gg 1$  limit in which all  $\cos(\cdot)$  factors average to zero except for one term for  $m = 1$  in which the  $\cos(0) = 1$ . Hence the incoherent limit of the  $n^{th}$  order in opacity induced radiation is

$$x \frac{dN_{in}^{(n)}}{dx d^2 \mathbf{k}} = \frac{C_R \alpha_s}{\pi^2} \frac{1}{n!} \int \prod_{i=1}^n \left( d^2 \mathbf{q}_i \left( \frac{L}{\lambda_g(i)} \right) [\bar{v}_i^2(\mathbf{q}_i) - \delta^2(\mathbf{q}_i)] \right) \left( -2 \tilde{\mathbf{C}}_{(1, \dots, n)} \cdot \tilde{\mathbf{B}}_{(2, \dots, n)(1, \dots, n)} \right) \quad , \quad (21)$$

For the  $n = 1$  contribution

$$\begin{aligned} x \frac{dN_{in}^{(1)}}{dx d^2 \mathbf{k}} &= \frac{C_R \alpha_s}{\pi^2} \left( \frac{L}{\lambda_g} \right) \int d^2 \mathbf{q}_1 [\bar{v}^2(\mathbf{q}_1) - \delta^2(\mathbf{q}_1)] \left( -2 \tilde{\mathbf{C}}_{(1)} \cdot \tilde{\mathbf{B}}_{(0)(1)} \right) \\ &= \frac{C_R \alpha_s}{\pi^2} \left( \frac{L}{\lambda_g} \right) \int d^2 \mathbf{q}_1 \bar{v}^2(\mathbf{q}_1) \left( \tilde{\mathbf{B}}_{(0)(1)}^2 + \tilde{\mathbf{C}}_{(1)}^2 - \tilde{\mathbf{H}}^2 \right) \quad , \end{aligned} \quad (22)$$

where  $\tilde{\mathbf{B}}_{(0)(1)} = \tilde{\mathbf{H}} - \tilde{\mathbf{C}}_{(1)}$  is the finite mass generalization of the incoherent GB radiation amplitude including the asymptotic plasmon dispersion. Note that (see Wiedemann [14]) the  $-\tilde{\mathbf{H}}^2$  term corresponds to the first order unitarity correction of the full Glauber *associated* zeroth order in opacity contribution  $e^{-L/\lambda_g} dN^{(0)}/dx d^2 \mathbf{k}$ . In addition elastic rescattering of the radiated gluon leads to the cascade contribution  $\tilde{\mathbf{C}}_{(1)}^2$  which further broadens the (already very broad) transverse momentum distribution of the associated radiation. The incoherent induced radiation from the rescattering of the quark jet in the medium is the Gunion-Bertsch term  $\tilde{\mathbf{B}}_{(0)(1)}^2$ . There are  $L/\lambda_g$  such induced contributions in the completely incoherent limit.

In general we expect that with the inclusion of masses in Eq.(15), the increase of the  $\Omega_{(m, \dots, n)} \Delta z_m$  arguments of the interference cosines in Eq.(17) will drive the radiation distribution closer to the incoherent limit. In the next section we will evaluate numerically how close is charm and bottom quark induced radiation to their respective incoherent limits.

Similar to the massless case studied in GLV [16], we expect that in the case of finite mass, higher orders in opacity contributions to the net induced energy loss will converge rapidly for moderate  $L/\lambda_g$  of practical interest. The dominance of the first order contribution to the transverse momentum integrated energy loss is more readily seen in the incoherent limit above. Change variables  $\mathbf{k} \rightarrow \mathbf{k}' \equiv \mathbf{k} - \mathbf{q}_2 - \cdots - \mathbf{q}_n$  and integrate over  $\mathbf{k}'$ . In the  $\omega \gg \mu$  limit, we can approximately ignore the change in the  $|\mathbf{k}'| < \omega$  kinematic limit. In that case

$$\int d^2 \mathbf{k} \tilde{\mathbf{C}}_{(1, \dots, n)} \cdot \tilde{\mathbf{B}}_{(2, \dots, n)(1, \dots, n)} \approx \int d^2 \mathbf{k}' \tilde{\mathbf{C}}_{(1)} \cdot \tilde{\mathbf{B}}_{(0)(1)} \quad . \quad (23)$$

However, the integrated energy loss at order  $n \geq 2$  has additional integrations

$$\int \prod_{i=2}^n d^2 \mathbf{q}_i [\bar{v}_i^2(\mathbf{q}_i) - \delta^2(\mathbf{q}_i)] = 0$$

that tend to kill the whole contribution modulo tiny edge effects due to Eq.(23) not being exact. Therefore, especially as we approach the incoherent limit the main order contribution to the medium induced energy loss is dominated by the first order in opacity.

In order to see how this works in more detail consider the case of uncorrelated geometries where we can use Eq.(20) and Fourier techniques to sum the whole opacity series in this incoherent limit. Note first that the term proportional to  $\delta^2(\mathbf{q}_1)$  vanishes due to  $\tilde{\mathbf{B}}_{(2,\dots,n)(1,\dots,n)} = 0$  when  $\mathbf{q}_1 = 0$ . It is convenient therefore to define the accumulated  $\mathbf{Q} = \sum_2^n \mathbf{q}_i$  momentum transfer distribution by inserting a factor

$$1 = \int d^2 \mathbf{Q} \delta^2(\mathbf{Q} - \sum_{i=2}^n \mathbf{q}_i) = \int \frac{d^2 \mathbf{Q}}{(2\pi)^2} \int d^2 \mathbf{b} e^{i\mathbf{Q}\cdot\mathbf{b}} \prod_{i=2}^n e^{-i\mathbf{q}_i\cdot\mathbf{b}}$$

Define an effective dipole cross section

$$\sigma_d(z, \mathbf{b}) \equiv - \int d^2 \mathbf{q} e^{-i\mathbf{q}\cdot\mathbf{b}} (\sigma(z_i, \mathbf{q}_i) - \sigma_{el}(z)\delta^2(\mathbf{q}_i))$$

and a corresponding dipole opacity

$$\chi_d(z, \mathbf{b}) \equiv \rho(z_i)\sigma_d(z, \mathbf{b}).$$

In terms of these quantities,

$$\begin{aligned} x \frac{dN_{in}^{(n)}}{dx d^2 \mathbf{k}} &= \frac{C_R \alpha_s}{\pi^2} \int_0^\infty dz_1 d^2 \mathbf{q}_1 \rho(z_1) \sigma(z_1, \mathbf{q}_1) \\ &\int \frac{d^2 \mathbf{Q}}{(2\pi)^2} \int d^2 \mathbf{b} e^{i\mathbf{Q}\cdot\mathbf{b}} \int_{z_1}^\infty dz_2 (-1) \chi_d(z_2, b) \int_{z_3}^\infty \dots \int_{z_{n-1}}^\infty dz_n (-1) \chi_d(z_n, b) \times \\ &\quad \times 2 \tilde{\mathbf{C}}_{\mathbf{k}-\mathbf{Q}-\mathbf{q}_1} \cdot (\tilde{\mathbf{C}}_{\mathbf{k}-\mathbf{Q}-\mathbf{q}_1} - \tilde{\mathbf{C}}_{\mathbf{k}-\mathbf{Q}}) \\ &= \frac{C_R \alpha_s}{\pi^2} \int_0^\infty dz_1 d^2 \mathbf{q}_1 \rho(z_1) \sigma(z_1, \mathbf{q}_1) \\ &\int \frac{d^2 \mathbf{Q}}{(2\pi)^2} \int d^2 \mathbf{b} e^{i\mathbf{Q}\cdot\mathbf{b}} \frac{(-1)^{n-1}}{(n-1)!} \left( \int_{z_1}^\infty dz_2 \chi_d(z_2, b) \right)^{n-1} \times \\ &\quad \times 2 \tilde{\mathbf{C}}_{\mathbf{k}-\mathbf{Q}-\mathbf{q}_1} \cdot (\tilde{\mathbf{C}}_{\mathbf{k}-\mathbf{Q}-\mathbf{q}_1} - \tilde{\mathbf{C}}_{\mathbf{k}-\mathbf{Q}}) \end{aligned} \quad (24)$$

We can now sum all orders from  $n = 1, \infty$  into a closed form

$$\begin{aligned} x \frac{dN_{in}}{dx d^2 \mathbf{k}} &= \frac{C_R \alpha_s}{\pi^2} \int_0^\infty dz_1 d^2 \mathbf{q}_1 \rho(z_1) \sigma(z_1, \mathbf{q}_1) \\ &\int \frac{d^2 \mathbf{Q}}{(2\pi)^2} \left[ \int d^2 \mathbf{b} e^{i\mathbf{Q}\cdot\mathbf{b}} e^{-\int_{z_1}^\infty dz' \rho(z') \sigma_d(z', b)} \right] \times \\ &\quad \times 2 \tilde{\mathbf{C}}_{\mathbf{k}-\mathbf{Q}-\mathbf{q}_1} \cdot (\tilde{\mathbf{C}}_{\mathbf{k}-\mathbf{Q}-\mathbf{q}_1} - \tilde{\mathbf{C}}_{\mathbf{k}-\mathbf{Q}}) \end{aligned} \quad (25)$$

We can now clearly see how (25) reduces to the first order result when integrated over  $\mathbf{k}$ . If we change variables to  $\mathbf{k}' = \mathbf{k} - \mathbf{Q}$  and assume that  $k' < \omega$  remains approximately valid, then the  $\mathbf{Q}$  integration reduces



to a  $\delta^2(\mathbf{b})$  which in turn converts  $\sigma_d(z, b) \rightarrow \sigma_d(z, 0) = 0$ . The whole second line reduces then to a unit factor so that

$$x \frac{dN_{in}}{dx} \approx \frac{C_R \alpha_s}{\pi^2} \int_0^\infty dz d^2 \mathbf{q} \rho(z) \sigma(z, \mathbf{q}) \int d^2 \mathbf{k} 2 \tilde{\mathbf{C}}_{\mathbf{k}-\mathbf{q}_1} \cdot (\tilde{\mathbf{C}}_{\mathbf{k}-\mathbf{q}_1} - \tilde{\mathbf{H}}) \quad (26)$$

However, in the same approximation that led to (26) from (25), we can again shift variables to  $\mathbf{k}' = \mathbf{k} - \mathbf{q}_1$  and again neglect the change in the  $|k'| < \omega$  bound to cancel the  $\tilde{\mathbf{C}}^2 - \tilde{\mathbf{H}}^2$  contribution. This collapses the full result to the simple incoherent Gunion-Bertsch limit

$$x \frac{dN_{in}}{dx} \approx x \frac{dN_{GB}}{dx} = \frac{C_R \alpha_s}{\pi^2} \int_0^\infty dz d^2 \mathbf{q} \rho(z) \sigma(z, \mathbf{q}) \int d^2 \mathbf{k} \tilde{\mathbf{B}}_{(0)(1)}^2 \quad (27)$$

In order to assess the accuracy of the approximations involved in the approximate handling of the kinematic  $k$  bounds, we have to evaluate numerically the difference between  $dN_{in}$  and  $dN_{BG}$ .

## 5 Numerical estimates

### 5.1 Heavy quark energy loss at RHIC

The numerical results for the first order induced radiative energy loss are shown on Fig.1 for charm and bottom quarks. From the analysis of light quark quenching in  $Au + Au$  at 130 GeV [36] effective static plasma opacity  $L/\lambda$  is in the range 3 – 4. On Fig.1 we fix opacity to  $L/\lambda = 4$ , and we look at the 1<sup>st</sup> order in opacity fractional energy loss as a function of initial energy of the quark. We assume here that  $\alpha_s = 0.3$ ,  $\mu = 0.5$  GeV, and  $\lambda = 1$  fm for the plasma parameters. Since finite parton masses shield collinear  $\mathbf{k} \rightarrow 0$  singularity [33], our numerical computations are performed with zero momentum cutoff. We see that for heavy quarks, in the energy range  $E \sim 5 - 15$  GeV, the Ter-Mikayelian effect reduces the induced energy loss in this extension of the GLV approach somewhat more than in the BDMS approximation [29]. However, on an absolute scale, this only corresponds to a change of  $\delta(\Delta E^{(1)}/E) < 0.05$ , which is negligible. Note that with both dead cone and plasmon mass reduction, there remains a sizeable induced energy loss fraction  $\Delta E^{(1)}/E \approx 0.15$  for charm quarks while only about half that is predicted for bottom.

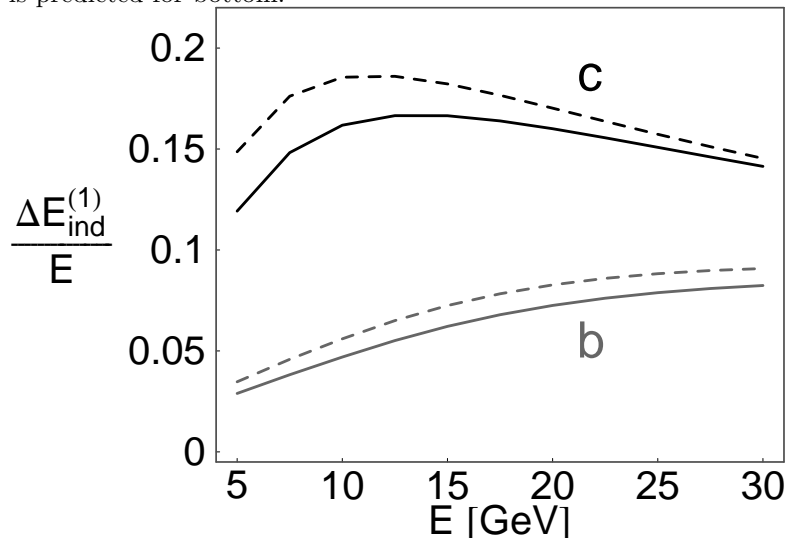


FIG 1. The 1<sup>st</sup> order in opacity fractional energy loss for heavy quarks with (solid curves) and without (dashed curves) Ter-Mikayelian effect approximated by a constant  $m_g = \mu/\sqrt{2}$  for transverse modes only. Upper curves correspond to charm, and lower to bottom quarks as a function of their energy in a plasma characterized by  $\alpha_s = 0.3$ ,  $\mu = 0.5$  GeV, and  $L = 4\lambda = 4$  fm.

However, we want to emphasize that, though Ter-Mikayelian effect is not important for the medium induced energy loss of the massive quarks, it is very important for massless quark case. Note that excluding Ter-Mikayelian effect means setting both plasmon mass and momentum cutoff to zero. Since in the massless parton case,  $\mathbf{k} \rightarrow 0$  singularities are not naturally regulated, excluding the Ter-Mikayelian effect would lead to infinite result of medium induced energy loss. In [16] these divergences are prevented by introducing the finite  $|\mathbf{k}| > \mu$  cutoff. It is easy to see from numerical computations that medium induced energy loss for light quarks with finite plasmon mass  $m_g = \mu/\sqrt{2}$  and zero momentum cutoff, is similar to the energy loss obtained with zero plasmon mass and finite momentum cutoff  $|\mathbf{k}| > \mu$ . Setting the finite momentum cutoff [16] in the case of light partons thus numerically produces similar results as introducing the finite plasmon mass, i.e. including the Ter-Mikayelian effect. Therefore, though the Ter-Mikayelian effect was not considered in [16], the same effect was obtained by including the finite momentum cutoff. However, we would like to note that, though both approaches give similar numerical results, the advantage of the Ter-Mikayelian effect is that it provides the natural regulation of  $\mathbf{k} \rightarrow 0$  divergences.

Fig. 2 shows the first order induced radiative energy loss for charm and bottom quarks as a function of opacity. We see that the induced contribution increases with  $L$ . Note that for heavy (charm and bottom) quarks the thickness dependence is closer to the linear Bethe-Heitler like form,  $L^1$ , than the asymptotic energy quadratic form [14, 16].

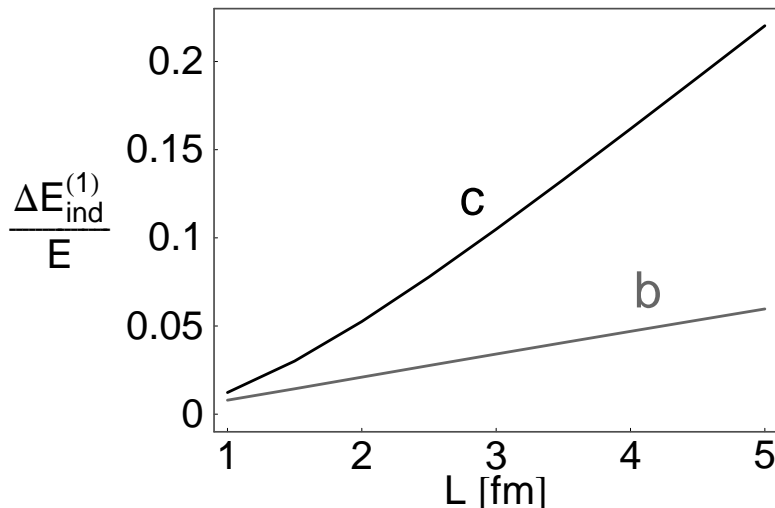


FIG 2. The 1<sup>st</sup> order in opacity fractional energy loss for a 10 GeV charm and bottom quark is plotted versus the effective static thickness  $L$  of a plasma characterized by  $\mu = 0.5$  GeV and  $\lambda = 1$  fm. Upper curve correspond to charm, and lower to bottom quark.

In the case of finite kinematic bounds on  $|\mathbf{q}_1| < \sqrt{6ET}$ , the angular integration in Eq. (11) can still be performed, but the result is cumbersome. However, including finite kinematic bound on  $|\mathbf{q}_1|$  is found to be unimportant, because it only reduces the induced energy loss fraction  $\Delta E^{(1)}/E$  in Fig. 1 by less than 10%. Therefore, we can safely neglect the finite kinematic boundaries on the momentum transfers.

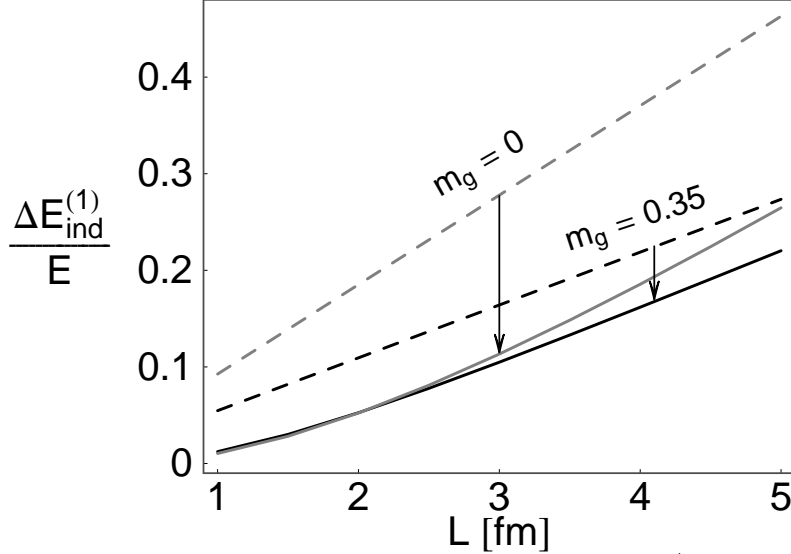


FIG 3. Comparison of the incoherent limit (dashed curves) to the 1<sup>st</sup> order (solid curves) in opacity fractional energy loss for  $E = 10$  GeV charm quarks via Eq. (12) under RHIC conditions ( $\alpha_s = 0.3$ ,  $\mu = 0.5$  GeV). The higher dashed and solid curves correspond to  $m_g = 0$ , while the lower to  $m_g = \mu/\sqrt{2}$ . Arrows point between corresponding incoherent limit and full 1<sup>st</sup> order results.

In Fig. 3 the first order energy loss for charm quarks is compared to the incoherent limit obtained from Eq.(12) by setting  $4xE/L = 0$ . This analogue of the QED Bethe-Heitler limit is the one where no destructive LPM interference effects occur in QCD. The characteristic of the incoherent limit is the complete linear dependence of  $\Delta E$  on  $L$ . The slope depends on the assumed  $\mu$  as well as the assumed dynamical gluon mass. Two cases,  $m_g = 0, \mu/\sqrt{2}$  are shown by the two dashed lines. Comparing to the solid lines that include destructive interference effects due to finite formation times, we see that the realistic case with finite  $m_g = 0.35$  GeV is remarkably close to the incoherent limit for  $E = 10$  GeV quarks.

We have also checked numerically the difference between the full first order incoherent limit and the isolated Gunion-Bertsch contribution. These should be approximately the same if the elastic rescattering and the hard unitarity correction terms cancel as in Eq.(27). We find that the GB energy loss for  $E=10$  GeV charm quarks is  $\Delta E_{GB}/E \approx 0.35$  is significantly larger than the incoherent energy loss  $\Delta E_{in}/E \approx 0.22$ . However by  $E = 30$  GeV, the GB limit exceeds the incoherent limit by only 15%.

Finally, by using the results for associated energy loss from [33], we can now compare the net  $(\Delta E_{ind}^{(1)} + \Delta E_{med}^{(0)})$  energy loss in the medium, with the one in the vacuum defined by  $\mu_{vac} = 0$  GeV, as shown on Fig. 4. As in paper I, we see that even in the absence of a medium ( $L = 0$ ), a charm quark with energy  $\sim 10$  GeV suffers an average energy loss,  $\Delta E_{vac}^{(0)}/E \approx 1/3$ , due to the sudden change of the color current when it is formed in the vacuum. The dielectric plasmon effect reduces this to about  $\Delta E_{med}^{(0)}/E \approx 1/4$ . This contribution is independent of the thickness of the plasma as long as  $L$  is not too small. For very small  $L < 1/m_g$ , the plasmon dispersion is smeared out due to the uncertainty principle, and  $\Delta E_{med}^{(0)}$  must approach  $\Delta E_{vac}^{(0)}$  from below.

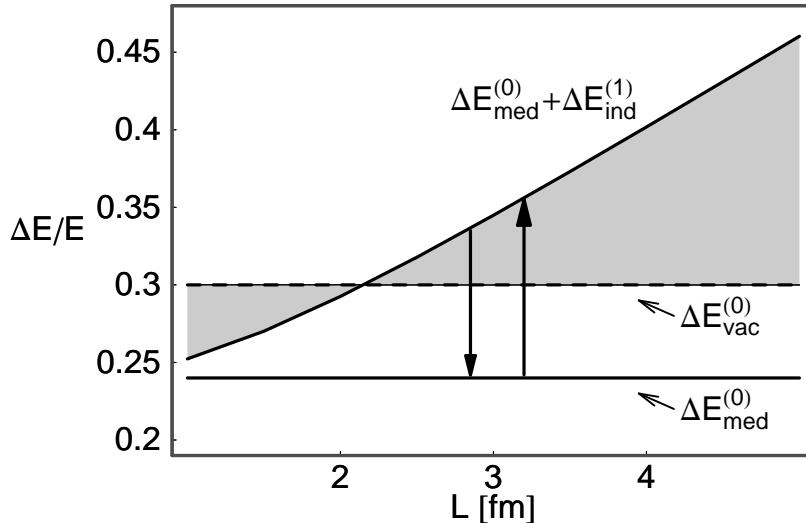


FIG 4. The fractional energy loss for a 10 GeV charm quark is plotted versus the effective static thickness  $L$  of a plasma characterized by  $\mu = 0.5$  GeV and  $\lambda = 1$  fm. The dashed middle horizontal line corresponds to the energy loss in the vacuum taking into account the kinematic dead cone of radiation for heavy quarks [29]. The lower horizontal solid line shows our estimate of the reduction of the zeroth order energy loss due to the QCD analog of the Ter-Mikayelian effect. The solid curve corresponds to the net energy loss,  $\Delta E_{med}^{(0)} + \Delta E_{ind}^{(1)}$ .

We see that the net energy loss,  $\Delta E_{med}^{(0)} + \Delta E_{ind}^{(1)}$ , is found to be even smaller than in [33] due to the corrections made in Eq. (12). Also, notice that for the effective static opacity medium [36] with  $L$  in the range of 3 – 4 fm,  $\mu \approx 0.5$  GeV and  $\lambda \approx 1$  fm, the difference between the medium energy loss ( $\Delta E_{med}^{(0)} + \Delta E_{ind}^{(1)}$ ) and naive vacuum value ( $\Delta E_{vac}^{(0)}$ ) is small, i.e. between 5% and 10% of the initial energy of the quark. These results, therefore, suggest that in addition to the heavy quark dead cone effect, the apparent null effect observed for heavy quark energy loss via single electrons may in part be due to a further reduction of the leading order energy loss. The different dependence of these effects on the plasma thickness  $L$  and on the transport properties,  $\mu$  and  $\lambda$ , should make it possible to test this explanation by varying the beam energy,  $A$ , and centrality at RHIC and LHC energies.

## 5.2 Heavy quark energy loss at LHC

In this section we want to estimate the heavy quark energy loss at LHC. According to some estimates [8], the density of plasma partons at LHC should be 3-4 times larger than the one at RHIC. Therefore the results below are calculated using  $\lambda$  and  $\mu$  based on the estimate given above.

The numerical results for the first order induced radiative energy loss are shown on Fig.5 for charm and bottom quarks. We assume here that  $\alpha_s = 0.3$ ,  $\mu = 0.7$  GeV,  $\lambda = 0.7$  fm and  $L = 4$  fm for the plasma parameters. As before, the Ter-Mikayelian effect does not have significant effect on the induced energy loss. On the other hand, we see that the induced energy loss fraction is two times larger than before, i.e.  $\Delta E^{(1)}/E \approx 0.3$  for charm quarks and about half for bottom.

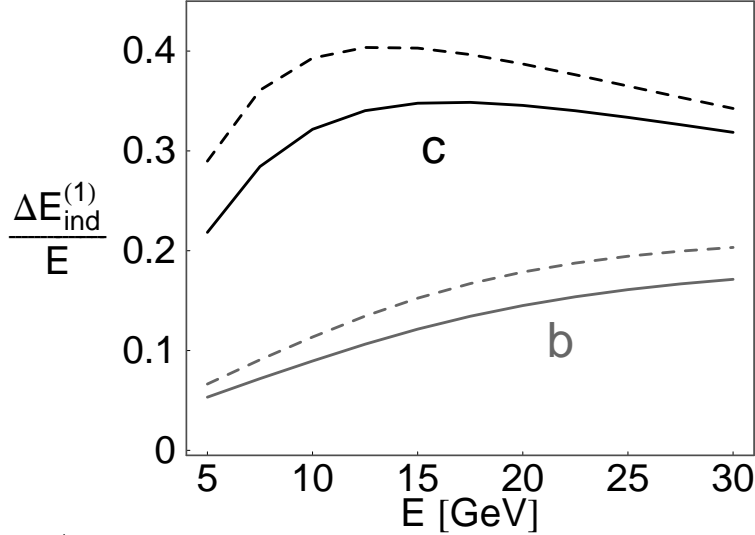


FIG 5. The 1<sup>st</sup> order in opacity fractional energy loss for heavy quarks with (solid curves) and without (dashed curves) Ter-Mikayelian effect approximated by a constant  $m_g = \mu/\sqrt{2}$  for transverse modes only. Upper curves correspond to charm, and lower to bottom quarks as a function of their energy in a plasma characterized by  $\alpha_s = 0.3$ ,  $\mu = 0.7$  GeV,  $\lambda = 0.7$  fm and  $L = 4$  fm.

Fig. 6 shows the first order induced radiative energy loss for charm and bottom quarks as a function of opacity. We see that, again, for bottom quarks the thickness dependence is still closer to the linear Bethe-Heitler like form,  $L^1$ , than the asymptotic energy quadratic form [14, 16]. However, for charm quark, the thickness dependence is somewhere between linear and quadratic form.

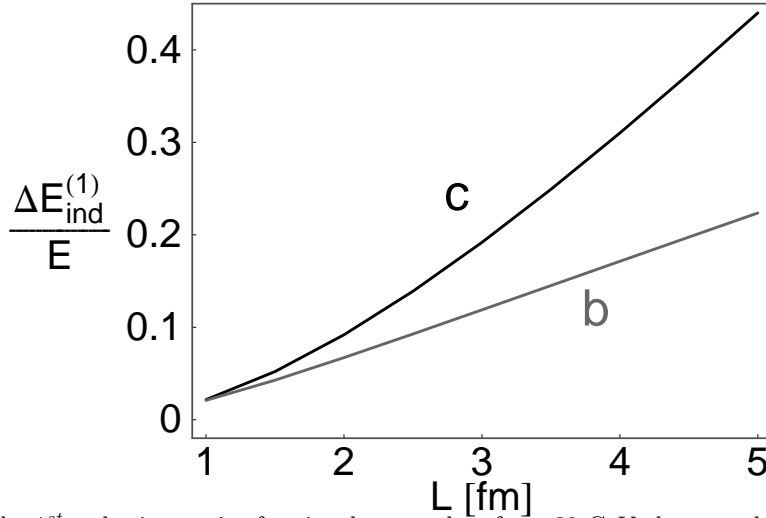


FIG 6. The 1<sup>st</sup> order in opacity fractional energy loss for a 30 GeV charm and bottom quark is plotted versus the effective static thickness  $L$  of a plasma characterized by  $\mu = 0.7$  GeV and  $\lambda = 0.7$  fm. Upper curve correspond to charm, and lower to bottom quark.

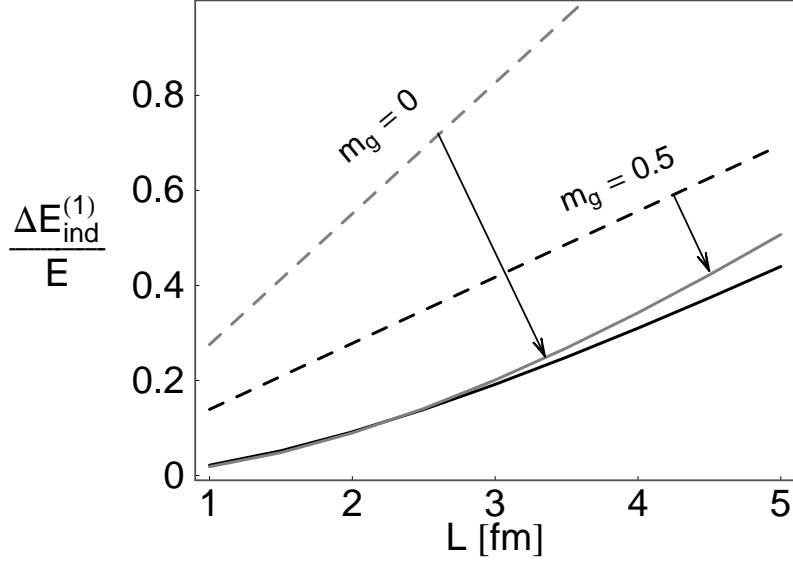


FIG 7. Comparison of the incoherent limit (dashed curves) to the 1<sup>st</sup> order (solid curves) in opacity fractional energy loss for  $E = 30$  GeV charm quarks via Eq.(12) under estimated LHC conditions ( $\alpha_s = 0.3$ ,  $\mu = 0.7$  GeV). As in Fig. 3, the higher dashed and solid curves correspond to  $m_g = 0$ , while the lower to  $m_g = \mu/\sqrt{2}$ . Arrows point between corresponding incoherent limit and full 1<sup>st</sup> order results.

Comparing Fig.7 to Fig. 3, we see that for 30 GeV quarks, the first order result is now further away from the incoherent limit. The destructive LPM finite formation effects included in the full 1<sup>st</sup> order result substantially reduce the incoherent energy loss.

For LHC conditions, we can again, by using the results for associated energy loss from [33], compare the net ( $\Delta E_{ind}^{(1)} + \Delta E_{med}^{(0)}$ ) energy loss in the medium, with the one in the vacuum defined by  $\mu_{vac} = 0$  GeV, as shown on Fig. 8. We see that the dielectric plasmon effect reduces the  $\Delta E_{med}^{(0)}/E$  from  $\approx 1/3$  to  $\approx 1/5$ . As before, this contribution is independent of the thickness of the plasma as long as  $L$  is not too small.

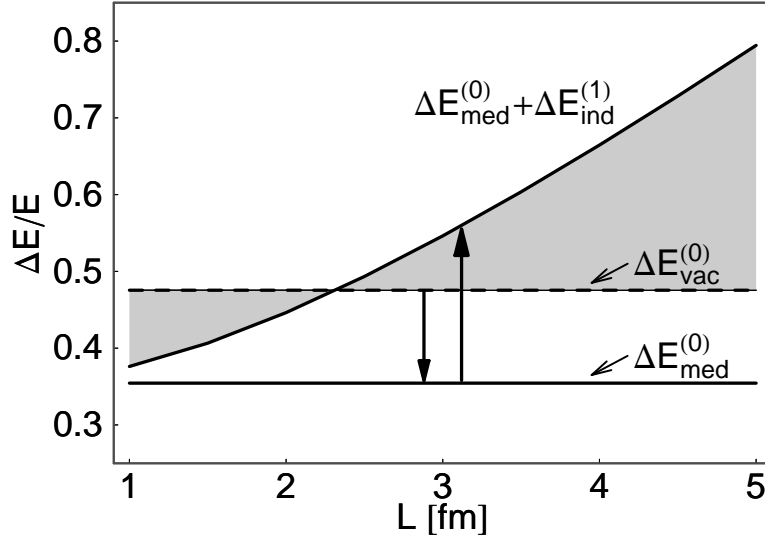


FIG 8. The fractional energy loss for a 30 GeV charm quark is plotted versus the effective static thickness  $L$  of a plasma characterized by  $\mu = 0.7$  GeV and  $\lambda = 0.7$  fm. The dashed middle horizontal line corresponds to the energy loss in the vacuum taking into account the kinematic dead cone of radiation for heavy quarks [29]. The lower horizontal solid line shows our estimate of the reduction of the zeroth order energy loss due to the QCD analog of the Ter-Mikayelian effect. The solid curve corresponds to the net energy loss,  $\Delta E_{med}^{(0)} + \Delta E_{ind}^{(1)}$ .

We see that the difference between net energy loss,  $\Delta E_{med}^{(0)} + \Delta E_{ind}^{(1)}$  and naive vacuum value  $\Delta E_{vac}^{(0)}$  at LHC is two times larger than the same difference at RHIC. Therefore, these results suggest a somewhat larger suppression of charm quark at LHC compared to RHIC.

## 6 Summary

In this paper we generalized the GLV radiative energy loss formalism to heavy quarks including also the plasmon effects. We have shown that the reaction operator method introduced in [16] can also be applied to the case of massive quarks and gluons. Remarkably, a simple mass dependent energy shift, via Eqs.(15,16), was found to modify all direct and virtual diagrams. This result, proven in the appendices A-G made it possible to generalize the GLV zero mass results to the case of heavy quarks to all orders in opacity. We also derived the incoherent limit of the induced radiation spectrum from heavy quarks and found a closed form expression summed to all orders in opacity.

The dependence of the charm first order in opacity energy loss on the jet energy and plasma parameters were studied numerically. We showed that the Ter-Mikayelian effect on the induced energy loss is comparable but somewhat larger than in [29]. In addition, it was shown that the induced contribution increases approximately linearly with  $L$ , as first reported in [33]. For charm quarks at RHIC the heavy quarks energy loss is close in magnitude and thickness dependence to the incoherent linear Bethe-Heitler like limit. This is in contrast to the quadratic (BDMS) thickness dependence characteristic for light quarks in the deep LPM regime. We note that ref. [34] reached similar conclusions using a different approach.

At LHC the partial LPM reduction of charm quark energy loss below the incoherent limit is predicted for  $E = 30$  GeV jets. However, the predictions for LHC are only quantitatively, but not qualitatively different from those at RHIC as long as the densities, and hence plasma parameters at LHC are not much more than about four times that at RHIC.

Finally we show in Fig. 9, the predicted radiation length (see Eq. (14)) as a function of the heavy quark mass under estimated RHIC and LHC quark gluon plasma conditions. The main feature to note is that the radiation length is comparable or greater than nuclear radii in all cases. The results imply that jet quenching is dominantly a volume emission rather than a surface emission phenomenon for all mass jets.

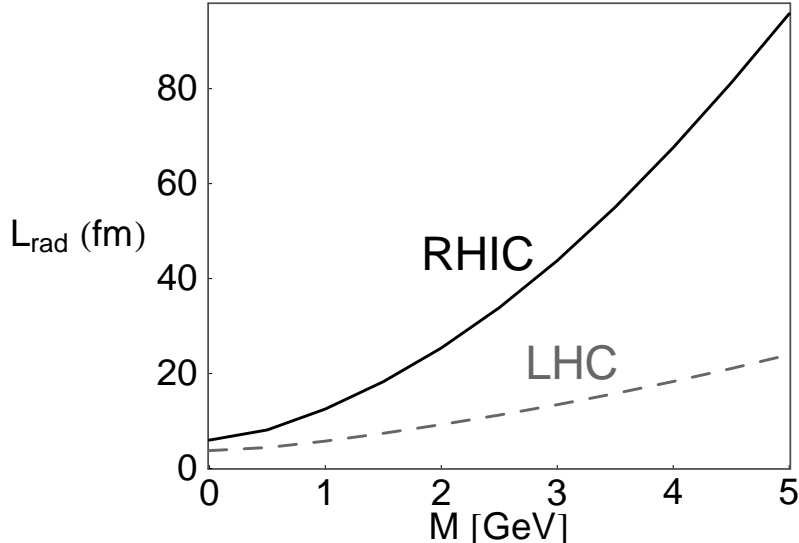


FIG 9. The radiation length of charm quarks as a function of their mass. Upper (lower) curve corresponds to the 10 (30) GeV charm quark at RHIC (LHC) conditions.

For light parton jets, the observed  $R_{AA} \sim 0.2$  accidentally suggest that only jets produced near the surface may survive to the detector. However, as shown in ref.[12], the finite GLV energy loss for jets propagating through the entire volume of the plasma quantitatively explains not only the magnitude and  $p_T$  dependence of  $R_{AA}(p_T)$  in central  $Au + Au$  but also its centrality dependence [39]. Heavy quark tomography will give an important complementary test of this physical picture. The computation presented here provides the basis for testing this theory on future experiments. The applications of heavy quark tomography to RHIC and LHC experiments is the subject of our current work.

*Acknowledgments:* Valuable discussions with I. Vitev, Z. Lin, J. Nagle, X.N. Wang, and W. Zajc on heavy quark production at RHIC are gratefully acknowledged. This work is supported by the Director, Office of Science, Office of High Energy and Nuclear Physics, Division of Nuclear Physics, of the U.S. Department of Energy under Grant No. DE-FG02-93ER40764.

## A Appendix: Assumptions

To compute the medium induced energy loss, we use the same assumptions as in [16]. For convenience, we recall here those assumptions.

First, we consider a Yukawa potential as in Eqs. (1) and assume that all the  $x_j$  are distributed with the same density

$$\rho(\vec{x}) = \frac{N}{A_{\perp}} \bar{\rho}(z) , \quad (28)$$

where  $\int dz \bar{\rho}(z) = 1$ .

Second, we assume that the observed  $p = [E^+, E^-, 0]$  is high as compared to the potential screening scale, i.e.



$$E^+ \gg \mu . \quad (29)$$

We also assume that the distance between the source and scattering centers are large compared to the interaction range

$$z_i - z_0 \gg 1/\mu . \quad (30)$$

Finally, we assume that the source current or packet  $J(p)$  varies slowly over the range of momentum transfers supplied by the potential.

A major simplification occurs if the relative transverse coordinate (impact parameter)  $\mathbf{b} = \mathbf{x}_i - \mathbf{x}_0$  varies over a large transverse area,  $A_\perp$ , relative to the interaction area  $1/\mu^2$ . In this case, the ensemble average over the scattering center location reduces to an impact parameter average as follows

$$\langle \dots \rangle = \int \frac{d^2\mathbf{b}}{A_\perp} \dots . \quad (31)$$

The ensemble average over the phase factor then yields

$$\langle e^{-i(\mathbf{q}-\mathbf{q}')\cdot\mathbf{b}} \rangle = \frac{(2\pi)^2}{A_\perp} \delta^2(\mathbf{q}-\mathbf{q}') \quad (32)$$

Also, to calculate the diagrams with one and two scattering centers we need to find the mass correction for the full triple gluon vertices  $\Lambda_i$ , and  $\Lambda_{ij}$  given in [16]. However, it is easy to show that in the approximation  $M^2/p_z^2 \ll 1$ , these vertices remain the same. Therefore, the full triple gluon vertices including coupling and color algebra for producing a final color  $c$  from initial color  $a$  followed by color potential interactions  $a_n$  and  $a_m$  are then given by

$$\begin{aligned} \Lambda_m &\equiv \Gamma_m(-f^{ca_m a})(ig_s t_a)(T_{a_m}(m)) \\ &\approx -2g_s E^+ \epsilon \cdot (\mathbf{k} - \mathbf{q}_m)[c, a_m] T_{a_m}(m) , \\ \Lambda_{mn} &\equiv \Gamma_{mn}(-f^{ca_n e})(-f^{ea_m a})(ig_s t_a)(T_{a_n}(n))(T_{a_m}(m)) \\ &\approx -2ig_s E^+ k^+ \epsilon \cdot (\mathbf{k} - \mathbf{q}_1 - \mathbf{q}_2)[[c, a_n], a_m](T_{a_n}(n)T_{a_m}(m)) . \end{aligned} \quad (33)$$

## B Diagrams $M_{1,0,0}$ , $M_{1,1,0}$ and $M_{1,0,1}$

In this appendix we present explicit calculation of the diagrams shown in Fig. 8.

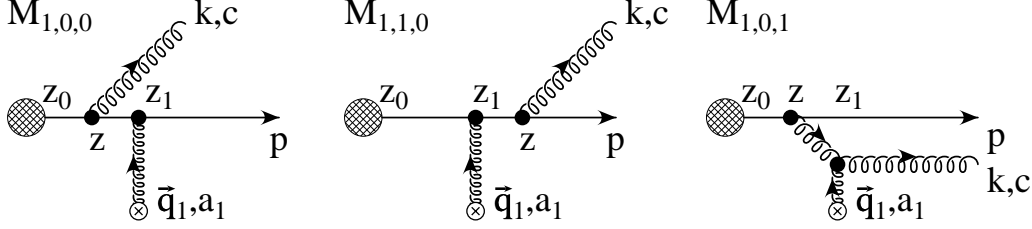


FIG 8. Three “direct” terms  $M_{1,0,0}$ ,  $M_{1,1,0}$  and  $M_{1,0,1}$  contribute to the soft gluon radiation amplitude to first order in opacity  $L/\lambda \propto \sigma_{el}/A_{\perp}$ .

### Computation of $M_{1,0,1}$

As a first application, consider the one rescattering amplitude  $M_{1,0,1}$ .

$$\begin{aligned}
M_{1,0,1} &= \int \frac{d^4 q_1}{(2\pi)^4} iJ(p+k-q_1) e^{i(p+k-q_1)x_0} \Lambda_1(p, k, q_1) V(q_1) e^{iq_1 x_1} \times \\
&\quad \times i\Delta_M(p+k-q_1) (-i)\Delta_{m_g}(k-q_1) \\
&\approx J(p+k) e^{i(p+k)x_0} [c, a_1] T_{a_1} (-i) \int \frac{d^2 \mathbf{q}_1}{(2\pi)^2} e^{-i\mathbf{q}_1 \cdot (\mathbf{x}_1 - \mathbf{x}_0)} 2g_s \epsilon \cdot (\mathbf{k} - \mathbf{q}_1) \times \\
&\quad \times 2E \int \frac{dq_{1z}}{2\pi} v(q_{1z}, \mathbf{q}_1) \Delta_M(p+k-q_1) \Delta_{m_g}(k-q_1) e^{-iq_{1z}(z_1-z_0)} .
\end{aligned} \tag{34}$$

The longitudinal momentum transfer integral,

$$I_1(p, k, \mathbf{q}_1, z_1 - z_0) \equiv \int \frac{dq_{1z}}{2\pi} v(q_{1z}, \mathbf{q}_1) \Delta_M(p+k-q_1) \Delta_{m_g}(k-q_1) e^{-iq_{1z}(z_1-z_0)} , \tag{35}$$

can be performed via closing the contour below the real axis since  $z_1 > z_0$ .

In addition to the potential singularities at  $\pm i\mu_1$  ( $\mu_i^2 \equiv \mu_{i\perp}^2 = \mathbf{q}_i^2 + \mu^2$ ), the two propagators have two poles in the lower  $q_{1z}$  plane, which are approximately located at

$$\begin{aligned}
\bar{q}_1 &= -\omega_0 - \tilde{\omega}_m - i\epsilon , \\
\bar{q}_2 &= -\omega_0 + \omega_1 - i\epsilon .
\end{aligned} \tag{36}$$

where  $\omega_0 = \frac{\mathbf{k}^2}{2\omega}$ ,  $\omega_i = \frac{(\mathbf{k}-\mathbf{q}_i)^2}{2\omega}$  and  $\tilde{\omega}_m = \frac{m_g^2 + M^2 x^2}{2\omega}$ . Note that  $\tilde{\omega}_m$  is the term which has the information on finite mass corrections.

The residues give

$$\begin{aligned}
\text{Res}(\bar{q}_1) &\approx -v(-\omega_0 - \tilde{\omega}_m, \mathbf{q}_1) \frac{e^{i(\omega_0 + \tilde{\omega}_m)(z_1 - z_0)}}{E^+ k^+ (\omega_1 + \tilde{\omega}_m)} , \\
\text{Res}(\bar{q}_2) &\approx v(\omega_1 - \omega_0, \mathbf{q}_1) \frac{e^{i(\omega_0 - \omega_1)(z_1 - z_0)}}{E^+ k^+ (\omega_1 + \tilde{\omega}_m)} ,
\end{aligned} \tag{37}$$

while

$$\text{Res}(-i\mu_1) \approx \frac{4\pi\alpha_s e^{-\mu_1(z_1-z_0)}}{(-2i\mu_1)E^+k^+(-i\mu_1)^2} , \quad (38)$$

where we assumed that  $k^+ \gg \mu_1 \gg \omega_i$ .

In the well-separated case where  $\mu(z_1 - z_0) = \mu\lambda \gg 1$ , this potential residue is exponentially suppressed and therefore

$$\begin{aligned} I_1(p, k, \mathbf{q}_1, z_1 - z_0) &\approx \frac{i}{E^+k^+(\omega_1 + \tilde{\omega}_m)} \times \\ &\times \left( v(-\omega_0 - \tilde{\omega}_m, \mathbf{q}_1) e^{i(\omega_0 + \tilde{\omega}_m)(z_1 - z_0)} - v(\omega_1 - \omega_0, \mathbf{q}_1) e^{i(\omega_0 - \omega_1)(z_1 - z_0)} \right) \\ &\approx v(0, \mathbf{q}_1) \frac{i}{E^+k^+(\omega_1 + \tilde{\omega}_m)} \left( e^{i(\omega_0 + \tilde{\omega}_m)(z_1 - z_0)} - e^{i(\omega_0 - \omega_1)(z_1 - z_0)} \right) . \end{aligned} \quad (39)$$

Using the fact that

$$\begin{aligned} \omega_0 + \tilde{\omega}_m &= \frac{\mathbf{k}^2 + m_g^2 + M^2 x^2}{2\omega} , \\ \omega_0 - \omega_1 &= \frac{\mathbf{k}^2 - (\mathbf{k} - \mathbf{q}_1)^2}{2\omega} \end{aligned} \quad (40)$$

we finally get

$$\begin{aligned} M_{1,0,1} &= J(p) e^{i(p+k)x_0} (-i) \int \frac{d^2\mathbf{q}_1}{(2\pi)^2} v(0, \mathbf{q}_1) e^{-i\mathbf{q}_1 \cdot \mathbf{b}_1} 2ig_s \frac{\epsilon \cdot (\mathbf{k} - \mathbf{q}_1)}{(\mathbf{k} - \mathbf{q}_1)^2 + M^2 x^2 + m_g^2} \times \\ &\times \left( e^{\frac{i}{2\omega}(\mathbf{k}^2 + m_g^2 + M^2 x^2)(z_1 - z_0)} - e^{\frac{i}{2\omega}(\mathbf{k}^2 - (\mathbf{k} - \mathbf{q}_1)^2)(z_1 - z_0)} \right) [c, a_1] T_{a_1} , \end{aligned} \quad (41)$$

where  $\mathbf{b}_1 = \mathbf{x}_1 - \mathbf{x}_0$ .

The Eq. (41) represents the massive corrections of Eq. (A7) in [16].

## Computation of $M_{1,0,0}$

Using the same technique as in the previous section we can now compute  $M_{1,0,0}$ .

$$\begin{aligned} M_{1,0,0} &= \int \frac{d^4 q_1}{(2\pi)^4} iJ(p+k-q_1) e^{i(p+k-q_1)x_0} (ig_s) \epsilon_\alpha (2p-2q_1+k)^\alpha \times \\ &\times i\Delta_M(p-q_1+k) i\Delta_M(p-q_1) (2p-q_1)^0 V(q_1) e^{iq_1 x_1} T_{a_1} a_1 c \\ &\approx J(p+k) e^{i(p+k)x_0} (-ig_s a_1 c T_{a_1}) 2E \int \frac{d^2\mathbf{q}_1}{(2\pi)^2} e^{-i\mathbf{q}_1 \cdot \mathbf{b}_1} I_2 , \end{aligned} \quad (42)$$

where

$$I_2(p, k, \mathbf{q}_1, z_1 - z_0) = \int \frac{dq_{z1}}{2\pi} \frac{\epsilon_\alpha (2p-2q_1+k)^\alpha}{(p-q_1+k)^2 - M^2 + i\epsilon} \frac{1}{(p-q_1)^2 - M^2 + i\epsilon} v(\bar{\mathbf{q}}_1) e^{-iq_{1z}(z_1-z_0)} . \quad (43)$$

Since  $z_1 > z_0$ , integral  $I_2$  can be performed via closing the contour below the real axis. Only roots  $(-\omega_0 - \tilde{\omega}_m - i\epsilon)$  and  $(\frac{\mathbf{q}_1^2}{2p_z} - i\epsilon)$  contribute to this integral (root  $-i\mu$  is suppressed, since  $\mu(z_1 - z_0) \gg 1$ ). Using the relations given in the Eq. (40) this integral becomes:

$$I_2(p, k, \mathbf{q}_1, z_1 - z_0) = \frac{i}{E} \frac{(\epsilon \cdot \mathbf{k})}{\mathbf{k}^2 + m_g^2 + M^2 x^2} v(0, \mathbf{q}_1) (e^{\frac{i}{2\omega}(\mathbf{k}^2 + m_g^2 + M^2 x^2)(z_1 - z_0)} - 1) \quad (44)$$

Finally  $M_{1,0,0}$  becomes

$$\begin{aligned} M_{1,0,0} &= J(p) e^{i(p+k)x_0} (-i) \int \frac{d^2 \mathbf{q}_1}{(2\pi)^2} v(0, \mathbf{q}_1) e^{-i\mathbf{q}_1 \cdot \mathbf{b}_1} (2ig_s) \times \\ &\times \frac{\epsilon \cdot \mathbf{k}}{\mathbf{k}^2 + m_g^2 + M^2 x^2} (e^{\frac{i}{2\omega}(\mathbf{k}^2 + m_g^2 + M^2 x^2)(z_1 - z_0)} - 1) a_1 c T_{a_1}. \end{aligned} \quad (45)$$

### Computation of $M_{1,1,0}$

$$\begin{aligned} M_{1,1,0} &= \int \frac{d^4 q_1}{(2\pi)^4} iJ(p+k-q_1) e^{i(p+k-q_1)x_0} (2p+2k-q_1)^0 \times \\ &\times i\Delta_M(p-q_1+k) i\Delta_M(p+k) (ig_s) \epsilon_\alpha (2p+k)^\alpha V(q_1) e^{iq_1 x_1} T_{a_1} c a_1 \\ &\approx J(p+k) e^{i(p+k)x_0} (-ig_s T_{a_1} c a_1) (2E+2\omega) \int \frac{d^3 \mathbf{q}_1}{(2\pi)^3} e^{-i\bar{\mathbf{q}}_1(\bar{\mathbf{x}}_1 - \bar{\mathbf{x}}_0)} v(\bar{\mathbf{q}}_1) \times \\ &\times \frac{1}{(p-q_1+k)^2 - M^2 + i\epsilon} \frac{1}{(p+k)^2 - M^2 + i\epsilon} \epsilon_\alpha (2p+k)^\alpha \end{aligned} \quad (46)$$

Since  $\omega \ll E \implies (2E+2\omega) \approx 2E$ .

$$\frac{\epsilon_\alpha (2p+k)^\alpha}{(p+k)^2 - M^2 + i\epsilon} = \frac{2p\epsilon}{2pk+k^2} \quad (47)$$

In the large  $p_z$  limit this becomes

$$\frac{\epsilon_\alpha (2p+k)^\alpha}{(p+k)^2 - M^2 + i\epsilon} = 2\left(1 + \frac{M^2}{4p_z^2}\right) \frac{\epsilon \cdot \mathbf{k}}{\mathbf{k}^2 + m_g^2 + M^2 x^2} \approx 2 \frac{\epsilon \cdot \mathbf{k}}{\mathbf{k}^2 + x^2 M^2 + m_g^2} \quad (48)$$

Using these two results, we get

$$M_{1,1,0} = J(p) e^{ipx_0} (-ig_s) T_{a_1} c a_1 4E \frac{\epsilon \cdot \mathbf{k}}{\mathbf{k}^2 + m_g^2 + M^2 x^2} \int \frac{d^2 \mathbf{q}_1}{(2\pi)^2} e^{-i\mathbf{q}_1 \cdot \mathbf{b}_1} I_3(p, k, \mathbf{q}_1, z_1 - z_0) \quad (49)$$

where

$$\begin{aligned} I_3(p, k, \mathbf{q}_1, z_1 - z_0) &= \int \frac{dq_{z1}}{2\pi} \frac{1}{(p-q_1+k)^2 - M^2 + i\epsilon} e^{-iq_{z1}(z_1-z_0)} v(\bar{\mathbf{q}}_1) \\ &\approx (-i) \frac{e^{i(\omega_0 + \tilde{\omega}_m)(z_1 - z_0)}}{2p_z} v(0, \mathbf{q}_1) \end{aligned} \quad (50)$$

Therefore,

$$\begin{aligned}
M_{1,1,0} &= J(p)e^{i(p+k)x_0} (-i) \int \frac{d^2\mathbf{q}_1}{(2\pi)^2} v(0, \mathbf{q}_1) e^{-i\mathbf{q}_1 \cdot \mathbf{b}_1} \times \\
&\times (-2ig_s) \frac{\epsilon \cdot \mathbf{k}}{\mathbf{k}^2 + m_g^2 + M^2 x^2} e^{\frac{i}{2\omega}(\mathbf{k}^2 + m_g^2 + M^2 x^2)(z_1 - z_0)} ca_1 T_{a_1} , 
\end{aligned} \tag{51}$$

which in the massless limit,  $M = m_g = 0$ , leads to Eq. (A8) from [16].

## C Diagram $M_{2,0,3}$

Consider next the gluon two-scattering amplitude  $M_{2,0,3}$ . Fig. 9 shows that for inclusive processes two interesting cases arise.

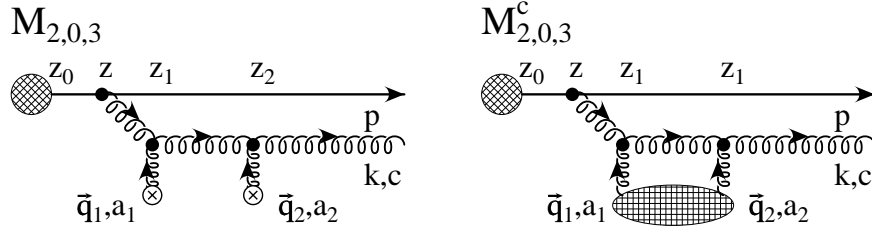


FIG 9.  $M_{2,0,3}$  “direct” contributes to second order in opacity  $\propto (\sigma_{el}/A_\perp)^2$ , whereas  $M_{2,0,3}^c = M_{2,0,3}(z_2 = z_1)$  “contact-limit” contribute to first order in opacity  $\propto (\sigma_{el}/A_\perp)^1$ .

In the Feynman diagram approach

$$\begin{aligned}
M_{2,0,3} &= \int \frac{d^4 q_1}{(2\pi)^4} \frac{d^4 q_2}{(2\pi)^4} iJ(p+k-q_1-q_2) e^{i(p+k-q_1-q_2)x_0} V(q_1) e^{iq_1 x_1} V(q_2) e^{iq_2 x_2} \times \\
&\times \Lambda_{12}(p, k, q_1, q_2) i\Delta_M(p+k-q_1-q_2) (-i)\Delta_{m_g}(k-q_1-q_2) (-i)\Delta_{m_g}(k-q_2) \\
&\approx J(p+k) e^{i(p+k)x_0} [[c, a_2], a_1] (T_{a_2}(2) T_{a_1}(1)) \times \\
&\times (-i) \int \frac{d^2 \mathbf{q}_1}{(2\pi)^2} (-i) \int \frac{d^2 \mathbf{q}_2}{(2\pi)^2} 2ig_s \epsilon \cdot (\mathbf{k} - \mathbf{q}_1 - \mathbf{q}_2) e^{-i\mathbf{q}_1 \cdot \mathbf{b}_1} e^{-i\mathbf{q}_2 \cdot \mathbf{b}_2} \times \\
&\times \int \frac{dq_{1z}}{(2\pi)} \frac{dq_{2z}}{(2\pi)} \frac{(4E\omega) v(\vec{\mathbf{q}}_1) v(\vec{\mathbf{q}}_2) e^{-iq_{1z}(z_1-z_0)} e^{-iq_{2z}(z_2-z_0)}}{((p+k-q_1-q_2)^2 + M^2 + i\epsilon)((k-q_1-q_2)^2 + m_g^2 + i\epsilon)((k-q_2)^2 + m_g^2 + i\epsilon)} \tag{52}
\end{aligned}$$

where  $\mathbf{b}_i = \mathbf{x}_i - \mathbf{x}_0$  are transverse impact parameters, and we used the soft gluon and rescattering kinematical simplifications Eqs. (33), e.g.  $J(p+k-q_1-q_2) \approx J(p+k) \approx J(p)$ . For the  $q_{1z}$  integral, it is convenient to rewrite the phase as

$$e^{-iq_{1z}(z_1-z_0)} e^{-iq_{2z}(z_2-z_0)} = e^{-i(q_{1z}+q_{2z})(z_1-z_0)} e^{-iq_{2z}(z_2-z_1)}.$$

The first longitudinal integral is closely related to Eq. (35)

$$I_2(p, k, \mathbf{q}_1, \bar{\mathbf{q}}_2, z_1 - z_0) = \int \frac{dq_{1z}}{2\pi} \frac{v(q_{1z}, \mathbf{q}_1) e^{-i(q_{1z} + q_{2z})(z_1 - z_0)}}{((p + k - q_1 - q_2)^2 + M^2 + i\epsilon)((k - q_1 - q_2)^2 + m_g^2 + i\epsilon)} . \quad (53)$$

Since  $z_1 - z_0 \gg 1/\mu$ , we again close the contour in the lower half  $q_{1z}$  plane and neglect the pole at  $-i\mu_1$ . The remaining  $q_{1z}$  poles are shifted by  $-q_{2z}$  and  $\mathbf{q}_1 \rightarrow \mathbf{q}_1 + \mathbf{q}_2$  relative to Eq. (36):

$$\begin{aligned} \bar{q}_1 &= -q_{2z} - \omega_0 - \tilde{\omega}_m - i\epsilon , \\ \bar{q}_2 &= -q_{2z} - \omega_0 + \omega_{(12)} - i\epsilon , \end{aligned} \quad (54)$$

where  $\omega_{(12)} = \frac{(\mathbf{k} - \mathbf{q}_1 - \mathbf{q}_2)^2}{2\omega}$ . The residues at  $\bar{q}_1, \bar{q}_2$  then give

$$I_2 \approx \frac{i \left( v(-q_{2z} - \omega_0 - \tilde{\omega}_m, \mathbf{q}_1) e^{i(\omega_0 + \tilde{\omega}_m)(z_1 - z_0)} - v(-q_{2z} - \omega_0 + \omega_{(12)}, \mathbf{q}_1) e^{i(\omega_0 - \omega_{(12)})(z_1 - z_0)} \right)}{E^+ k^+ (\omega_{(12)} + \tilde{\omega}_m)} , \quad (55)$$

where we have neglected  $\mathcal{O}(\exp(-\mu\lambda))$  contributions. This differs from Eq. (39) mainly in that the potential is evaluated near  $-q_{2z}$ , which still remains to be integrated over, and  $\omega_1 \rightarrow \omega_{(12)}$ .

Next we need the following *critical*  $q_{2z}$  integral

$$I_3(k, \mathbf{q}_1, \mathbf{q}_2, z_2 - z_1) \equiv \int \frac{dq_{2z}}{2\pi} \frac{v(-q_{2z} + \delta\omega, \mathbf{q}_1) v(q_{2z}, \mathbf{q}_2) e^{-iq_{2z}(z_2 - z_1)}}{((k - q_2)^2 + m_g^2 + i\epsilon)} . \quad (56)$$

In the general case (including the special contact case with  $z_2 = z_1$ ) both  $q_{2z} = -i\mu_2, -i\mu_1$  singularities in the Yukawa potential contribute together with the pole at  $q_{2z} = \omega_2 - \omega_0 - i\epsilon$ , resulting in

$$\begin{aligned} I_3(k, \mathbf{q}_1, \mathbf{q}_2, z_2 - z_1) \approx & \frac{-i}{k^+} \left[ v(0, \mathbf{q}_1) v(0, \mathbf{q}_2) e^{-i(\omega_2 - \omega_0)(z_2 - z_1)} \right. \\ & \left. - \frac{(4\pi\alpha_s)^2}{2(\mu_1^2 - \mu_2^2)} \left( \frac{e^{-\mu_2(z_2 - z_1)}}{\mu_2^2} - \frac{e^{-\mu_1(z_2 - z_1)} e^{-i\delta\omega(z_2 - z_1)}}{\mu_1^2} \right) \right] . \end{aligned} \quad (57)$$

Fortunately, we are interested in only two extreme limits:

- The limit of well-separated scattering centers  $z_2 - z_1 \gg 1/\mu$  ;
- The special “contact”  $z_2 = z_1$  limit to compute unitary contributions.

For  $z_2 - z_1 = \lambda \gg 1/\mu$  the Eq. (57) reduces to

$$I_3(k, \mathbf{q}_1, \mathbf{q}_2, z_2 - z_1 \gg 1/\mu) \approx -\frac{i}{k^+} v(0, \mathbf{q}_1) v(0, \mathbf{q}_2) e^{-i(\omega_2 - \omega_0)(z_2 - z_1)} . \quad (58)$$

For the special contact contribution  $z_2 - z_1 = 0$  it reduces to

$$I_3(k, \mathbf{q}_1, \mathbf{q}_2, 0) \approx \frac{-i}{2k^+} v(0, \mathbf{q}_1) v(0, \mathbf{q}_2) . \quad (59)$$

i.e., exactly  $\frac{1}{2}$  of the strength in Eq. (58).

The contact limit of this amplitude is therefore

$$\begin{aligned}
M_{2,0,3}^c &\approx J(p)e^{i(p+k)x_0}(-i) \int \frac{d^2\mathbf{q}_1}{(2\pi)^2} v(0, \mathbf{q}_1) e^{-i\mathbf{q}_1 \cdot \mathbf{b}_1}(-i) \int \frac{d^2\mathbf{q}_2}{(2\pi)^2} v(0, \mathbf{q}_2) e^{-i\mathbf{q}_2 \cdot \mathbf{b}_2} \times \\
&\times \frac{1}{2} (2ig_s) \frac{\epsilon \cdot (\mathbf{k} - \mathbf{q}_1 - \mathbf{q}_2)}{(\mathbf{k} - \mathbf{q}_1 - \mathbf{q}_2)^2 + M^2x^2 + m_g^2} [[c, a_2], a_1](T_{a_2}T_{a_1}) \times \\
&\times \left\{ e^{\frac{i}{2\omega}(\mathbf{k}^2 + m_g^2 + M^2x^2)(z_1 - z_0)} - e^{\frac{i}{2\omega}(\mathbf{k}^2 - (\mathbf{k} - \mathbf{q}_1 - \mathbf{q}_2)^2)(z_1 - z_0)} \right\}. \tag{60}
\end{aligned}$$

Note that in the massless limit it reduces to Eq. (B10) from [16].

## D Diagrams $M_{2,0,0}$ and $M_{2,2,0}$

In those graphs it is the jet rather than the gluon that suffers two sequential scatterings as seen from Fig. 10.

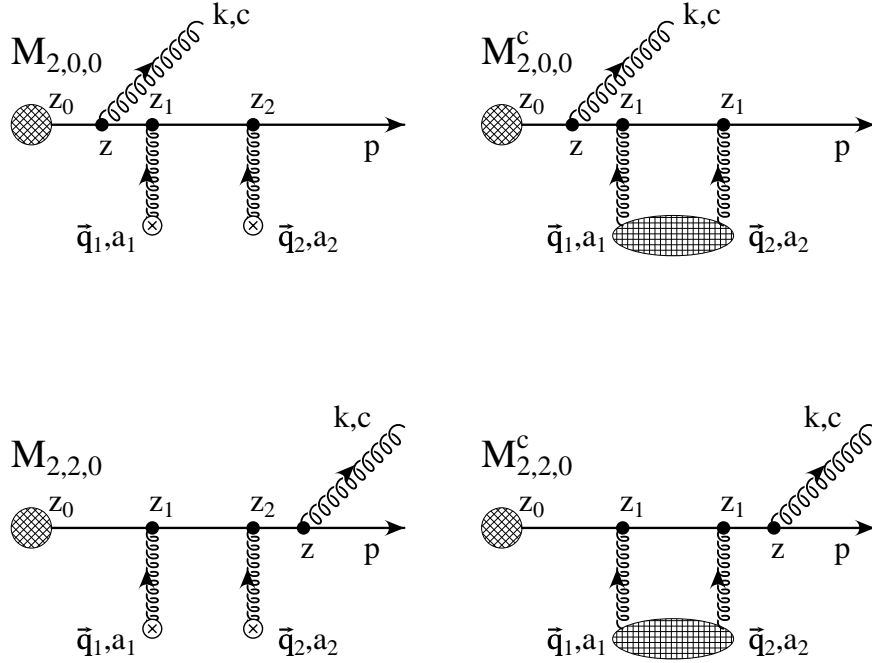


FIG 10.  $M_{2,0,0}$  and  $M_{2,2,0}$  graphs in the well-separated case together with their  $z_2 = z_1$  limits  $M_{2,0,0}^c$ ,  $M_{2,2,0}^c$ .

$$\begin{aligned}
M_{2,0,0} &= \int \frac{d^4q_1}{(2\pi)^4} \frac{d^4q_2}{(2\pi)^4} iJ(p+k-q_1-q_2)e^{i(p+k-q_1-q_2)x_0} V(q_1)e^{iq_1x_1} V(q_2)e^{iq_2x_2} \times \\
&\times (-i2E)^2 ig_s(2p+k)_\mu \epsilon^\mu i\Delta_M(p+k-q_1-q_2) i\Delta_M(p-q_1-q_2) i\Delta_M(p-q_2) a_2 a_1 c(T_{a_2}T_{a_1})
\end{aligned}$$

$$\begin{aligned}
&\approx J(p)e^{ipx_0}(-i) \int \frac{d^2\mathbf{q}_1}{(2\pi)^2} e^{-i\mathbf{q}_1 \cdot \mathbf{b}_1}(-i) \int \frac{d^2\mathbf{q}_2}{(2\pi)^2} e^{-i\mathbf{q}_2 \cdot \mathbf{b}_2} \frac{2ig_s(\boldsymbol{\epsilon} \cdot \mathbf{k})}{x} a_2 a_1 c(T_{a_2} T_{a_1}) (2E)^2 \times \\
&\times \int \frac{dq_{1z}}{(2\pi)} \frac{dq_{2z}}{(2\pi)} \frac{v(\bar{\mathbf{q}}_1)v(\bar{\mathbf{q}}_2)e^{-iq_{1z}(z_1-z_0)}e^{-iq_{2z}(z_2-z_0)}}{((p+k-q_1-q_2)^2+M^2+i\epsilon)((p-q_1-q_2)^2+M^2+i\epsilon)((p-q_2)^2+M^2+i\epsilon)} \quad (61)
\end{aligned}$$

In this case we define

$$I_2(p, k, \mathbf{q}_1, \bar{\mathbf{q}}_2, z_1 - z_0) = \int \frac{dq_{1z}}{2\pi} \frac{v(q_{1z}, \mathbf{q}_1)e^{-i(q_{1z}+q_{2z})(z_1-z_0)}}{((p+k-q_1-q_2)^2+M^2+i\epsilon)((p-q_1-q_2)^2+M^2+i\epsilon)} . \quad (62)$$

Since  $z_1 - z_0 \gg 1/\mu$ , we neglect the pole at  $-i\mu_1$ . The remaining  $q_{1z}$  poles are

$$\begin{aligned}
\bar{q}_1 &= -q_{2z} - \omega_0 - \tilde{\omega}_m - i\epsilon , \\
\bar{q}_2 &= -q_{2z} - i\epsilon ,
\end{aligned} \quad (63)$$

where we discarded  $(\mathbf{p} + \mathbf{k} - \mathbf{q}_1 - \mathbf{q}_2)^2/E^+$  relative to  $\omega_0$ . The  $\bar{q}_1, \bar{q}_2$  residues then give

$$I_2 \approx -i \frac{v(-q_{2z}, \mathbf{q}_1)}{(E^+)^2(\omega_0 + \tilde{\omega}_m)} \left( e^{i(\omega_0 + \tilde{\omega}_m)(z_1-z_0)} - 1 \right) . \quad (64)$$

Not that  $\omega_0$  has been neglected in the potential relative to  $\mu_1$ . In the contact limit, the second integral,  $I_3$ , is then equal to

$$\begin{aligned}
\bar{I}_3(p, \mathbf{q}_1, \mathbf{q}_2, z_2 - z_1) &\equiv \int \frac{dq_{2z}}{(2\pi)} \frac{v(-q_{2z}, \mathbf{q}_1)v(q_{2z}, \mathbf{q}_2)e^{-iq_{2z}(z_2-z_1)}}{((p-q_2)^2+M^2+i\epsilon)} \\
&\approx \frac{i}{E^+} v(0, \mathbf{q}_1)v(0, \mathbf{q}_2) \times \begin{cases} 1 & \text{if } \mu\lambda = \mu(z_2 - z_1) \rightarrow \infty \\ \frac{1}{2} & \text{if } \mu\lambda = \mu(z_2 - z_1) \rightarrow 0 \end{cases} . \quad (65)
\end{aligned}$$

With the help of Eqs. (64,65) in the case of contact limit we obtain

$$\begin{aligned}
M_{2,0,0}^c &= \frac{1}{2} J(p) e^{i(p+k)x_0} \int \frac{d^2\mathbf{q}_1}{(2\pi)^2} \frac{d^2\mathbf{q}_2}{(2\pi)^2} v(0, \mathbf{q}_1)v(0, \mathbf{q}_2) e^{-i(\mathbf{q}_1+\mathbf{q}_2) \cdot \mathbf{b}_1} \times \\
&\times (-2ig_s) \frac{(\boldsymbol{\epsilon} \cdot \mathbf{k})}{\mathbf{k}^2 + m_g^2 + M^2 x^2} \{ e^{\frac{i}{2\omega}(\mathbf{k}^2 + m_g^2 + M^2 x^2)(z_1-z_0)} - 1 \} a_2 a_1 c(T_{a_2} T_{a_1}) . \quad (66)
\end{aligned}$$

In the same way we will obtain for  $M_{2,2,0}$

$$\begin{aligned}
M_{2,2,0}^c &= \frac{1}{2} J(p) e^{i(p+k)x_0} \int \frac{d^2\mathbf{q}_1}{(2\pi)^2} \frac{d^2\mathbf{q}_2}{(2\pi)^2} v(0, \mathbf{q}_1)v(0, \mathbf{q}_2) e^{-i(\mathbf{q}_1+\mathbf{q}_2) \cdot \mathbf{b}_1} \times \\
&\times (2ig_s) \frac{(\boldsymbol{\epsilon} \cdot \mathbf{k})}{\mathbf{k}^2 + m_g^2 + M^2 x^2} e^{\frac{i}{2\omega}(\mathbf{k}^2 + m_g^2 + M^2 x^2)(z_1-z_0)} c a_2 a_1 (T_{a_2} T_{a_1}) . \quad (67)
\end{aligned}$$



## E Diagrams $M_{2,0,1}$ and $M_{2,0,2}$

Bellow we compute the case when one of the hits is on the parent parton and the other hit is on the radiated gluon. Explicit calculation is shown on the example of  $M_{2,0,1}^c = M_{2,0,1}(z_2 = z_1)$  in Fig. 11.

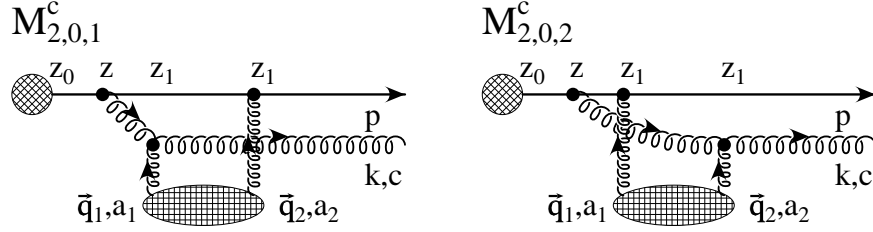


FIG 11.  $M_{2,0,1}^c$  and  $M_{2,0,2}^c$  topologically indistinct contact diagrams. There are no additional factors of  $\frac{1}{2}$  arising from the integration in taking the  $z_2 = z_1$  limit in  $M_{2,0,1}$  and  $M_{2,0,2}$ .

$$\begin{aligned}
M_{2,0,1} &= \int \frac{d^4 q_1}{(2\pi)^4} \frac{d^4 q_2}{(2\pi)^4} iJ(p+k-q_1-q_2) e^{i(p+k-q_1-q_2)x_0} V(q_1) e^{iq_1 x_1} V(q_2) e^{iq_2 x_2} \times \\
&\quad \times (-iE^+) \Lambda_1 i\Delta_M(p+k-q_1-q_2) (-i)\Delta_{m_g}(k-q_1) i\Delta_M(p-q_2) \\
&\approx J(p) e^{ipx_0} (-i) \int \frac{d^2 \mathbf{q}_1}{(2\pi)^2} e^{-i\mathbf{q}_1 \cdot \mathbf{b}_1} (-i) \int \frac{d^2 \mathbf{q}_2}{(2\pi)^2} e^{-i\mathbf{q}_2 \cdot \mathbf{b}_2} \times \\
&\quad \times 2ig_s(\epsilon \cdot (\mathbf{k} - \mathbf{q}_1)) e^{i\omega_0 z_0} a_2[c, a_1] (T_{a_2} T_{a_1}) (2E)^2 \times \\
&\quad \times \int \frac{dq_{1z}}{(2\pi)} \frac{dq_{2z}}{(2\pi)} \frac{v(\vec{\mathbf{q}}_1) v(\vec{\mathbf{q}}_2) e^{-iq_{1z}(z_1-z_0)} e^{-iq_{2z}(z_2-z_0)}}{((p+k-q_1-q_2)^2 + M^2 + i\epsilon)((k-q_1)^2 + m_g^2 + i\epsilon)((p-q_2)^2 + M^2 + i\epsilon)}. \quad (68)
\end{aligned}$$

We perform the  $q_{1z}$  integral first

$$I_2(p, k, \mathbf{q}_1, \vec{\mathbf{q}}_2, z_1 - z_0) = \int \frac{dq_{1z}}{2\pi} \frac{v(q_{1z}, \mathbf{q}_1) e^{-i(q_{1z} + q_{2z})(z_1 - z_0)}}{((p+k-q_1-q_2)^2 + M^2 + i\epsilon)((k-q_1)^2 + m_g^2 + i\epsilon)}. \quad (69)$$

The pole at  $-i\mu_1$  is again exponentially suppressed. The poles of interest in the lower half plane are  $q_{1z} = -q_{2z} - \omega_0 - \tilde{\omega}_m - i\epsilon$  and  $q_{1z} = -\omega_0 + \omega_1 - i\epsilon$ .

Taking the residues leaves us with

$$\begin{aligned}
I_2(p, k, \mathbf{q}_1, \vec{\mathbf{q}}_2, z_1 - z_0) &= \frac{i}{E^+ k^+ (q_{2z} + \omega_1 + \tilde{\omega}_m)} \times \\
&\quad \times \left( v(-q_{2z} - \omega_0 - \tilde{\omega}_m, \mathbf{q}_1) e^{i(\omega_0 + \tilde{\omega}_m)(z_1 - z_0)} - v(\omega_1 - \omega_0, \mathbf{q}_1) e^{i(\omega_0 - q_{2z} - \omega_1)(z_1 - z_0)} \right). \quad (70)
\end{aligned}$$

It is important to notice that there is no pole at  $q_{2z} = -\omega_1$  in Eq. (70). The remaining integral over  $q_{2z}$  is

$$\begin{aligned}
I_3(p, k, \mathbf{q}_1, \mathbf{q}_2, z_1 - z_0, z_2 - z_1) &= \int \frac{dq_{2z}}{2\pi} \frac{1}{q_{2z} + \omega_1 + \tilde{\omega}_m} \left( \frac{e^{-i(q_{2z}(z_2 - z_1) - (\omega_0 + \tilde{\omega}_m)(z_1 - z_0))}}{(p - q_2)^2 + M^2 + i\epsilon} \right) \times \\
&\times v(-q_{2z} - \omega_0 - \tilde{\omega}_m, \mathbf{q}_1) v(q_{2z}, \mathbf{q}_2) - \frac{e^{-i(q_{2z}(z_2 - z_0) + (\omega_1 - \omega_0)(z_1 - z_0))}}{(p - q_2)^2 + M^2 + i\epsilon} v(\omega_1 - \omega_0, \mathbf{q}_1) v(q_{2z}, \mathbf{q}_2). \quad (71)
\end{aligned}$$

The poles in the lower half plane are  $q_{2z} = -i\epsilon$ ,  $q_{2z} = -i\mu_2$ , and  $q_{2z} = -\omega_0 - \tilde{\omega}_m - i\mu_1$ . In the well separated case, contributions from second and third residue are exponentially suppressed  $\propto \exp[-\mu_2(z_1 - z_0)]$ , and therefore can be neglected. In the contact limit contributions from second and third residue cancel exactly (for more details see Eq. (d5) [16]). Therefore, we get

$$\begin{aligned}
M_{2,0,1}^c &= J(p) e^{i(p+k)x_0} (-i) \int \frac{d^2\mathbf{q}_1}{(2\pi)^2} e^{-i\mathbf{q}_1 \cdot \mathbf{b}_1} v(0, \mathbf{q}_1) (-i) \int \frac{d^2\mathbf{q}_2}{(2\pi)^2} e^{-i\mathbf{q}_2 \cdot \mathbf{b}_2} v(0, \mathbf{q}_2) \times \\
&\times 2ig_s \frac{\epsilon \cdot (\mathbf{k} - \mathbf{q}_1)}{(\mathbf{k} - \mathbf{q}_1)^2 + M^2 x^2 + m_g^2} \left\{ e^{i\left(\frac{\mathbf{k}^2 + m_g^2 + M^2 x^2}{2\omega} - q_{2z}\right)(z_1 - z_0)} - e^{i\frac{\mathbf{k}^2 - (\mathbf{k} - \mathbf{q}_1)^2}{2\omega}(z_1 - z_0)} \right\} a_2[c, a_1] (T_{a_2} T_{a_1}). \quad (72)
\end{aligned}$$

In the massless limit this equation reduces to Eq. (D6) from [16].

Notice that, unlike to the previous examples, there is no factor of  $\frac{1}{2}$  in  $M_{2,0,1}^c$ .

We can get  $M_{2,0,2}^c$  from  $M_{2,0,1}^c$  by replacing every 2 with 1 and *vice versa*.

However (since scattering centers are identical), we need to symmetrize this two diagrams, which effectively leads to multiplying every diagram with  $\frac{1}{2}$ .

## F Zero measure contact limit of $M_{2,1,0}$ and $M_{2,1,1}$

In calculating the different contributions coming from two interactions with the same potential centered around  $\bar{\mathbf{x}}_1$  we have to take into account the two graphs given in Fig. 12, where one of the hits occurs before the gluon emission vertex and the other one after.

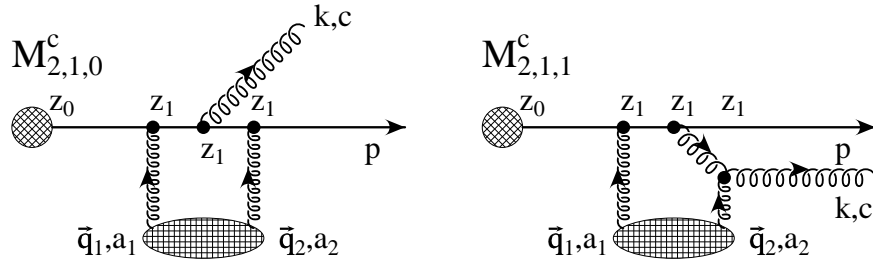


FIG 12. Diagrams  $M_{2,1,0}^c$  and  $M_{2,1,1}^c$  of  $\mathcal{O}(0)$  according to the time-ordered perturbation theory.

In the framework of time-ordered perturbation theory of [37, 38] the graphs are identically zero in the contact limit because  $\int_{t_1}^{t_1} dt \dots \equiv 0$ . Here we present a more detailed study of the validity of this argument in the case of massive quarks and gluons.

$$\begin{aligned}
M_{2,1,0} &= \int \frac{d^4 q_1}{(2\pi)^4} \frac{d^4 q_2}{(2\pi)^4} iJ(p+k-q_1-q_2) e^{i(p+k-q_1-q_2)x_0} \times \\
&\quad \times i\Delta_M(p+k-q_1-q_2)V(q_1)e^{iq_1x_1} i\Delta_M(p+k-q_2)(2p-2q_2+k)^\mu \epsilon_\mu i\Delta_M(p-q_2)ig_s V(q_2)e^{iq_2x_2} \times \\
&\quad \times (-i(2p+2k-q_1-2q_2)^0)(-i(2p-q_2)^0)a_2ca_1T_{a_2}T_{a_1} \\
&\approx J(p+k)e^{i(p+k)x_0} a_2ca_1(T_{a_2}T_{a_1})(-ig_s)(2E)^2 \times \\
&\quad \times \int \frac{d^3 \bar{\mathbf{q}}_1}{(2\pi)^3} \frac{d^3 \bar{\mathbf{q}}_2}{(2\pi)^3} v(\bar{\mathbf{q}}_1)e^{-i\bar{\mathbf{q}}_1(\bar{\mathbf{x}}_1-\bar{\mathbf{x}}_0)} v(\bar{\mathbf{q}}_2)e^{-i\bar{\mathbf{q}}_2(\bar{\mathbf{x}}_2-\bar{\mathbf{x}}_0)} (2p-2q_2+k)^\mu \epsilon_\mu \times \\
&\quad \times \Delta_M(p+k-q_1-q_2)\Delta_M(p+k-q_2)\Delta_M(p-q_2) \\
&= J(p+k)e^{i(p+k)x_0} a_2ca_1(T_{a_2}T_{a_1})(-ig_s)(2E)^2 \int \frac{d^2 \mathbf{q}_1}{(2\pi)^2} \frac{d^2 \mathbf{q}_2}{(2\pi)^2} e^{-i\mathbf{q}_1 \mathbf{b}_1} e^{-i\mathbf{q}_2 \mathbf{b}_2} \times \\
&\quad \times \int \frac{dq_{2z}}{2\pi} (2p-2q_2+k)^\mu \epsilon_\mu \frac{v(\bar{\mathbf{q}}_2)e^{-iq_{2z}(z_2-z_1)}}{((p-q_2)^2-M^2+i\epsilon)((p+k-q_2)^2-M^2+i\epsilon)} \int \frac{dq_z}{2\pi} \frac{v(q_z-q_{2z}, \mathbf{q}_1)e^{-iq_z(z_1-z_0)}}{((p+k-q)^2-M^2+i\epsilon)} \\
&= J(p+k)e^{i(p+k)x_0} a_2ca_1(T_{a_2}T_{a_1})(-ig_s)(2E)^2 \int \frac{d^2 \mathbf{q}_1}{(2\pi)^2} \frac{d^2 \mathbf{q}_2}{(2\pi)^2} e^{-i\mathbf{q}_1 \mathbf{b}_1} e^{-i\mathbf{q}_2 \mathbf{b}_2} \frac{\epsilon \cdot \mathbf{k}}{x} \times \\
&\quad \times \int \frac{dq_{2z}}{2\pi} \frac{v(\bar{\mathbf{q}}_2)e^{-iq_{2z}(z_2-z_1)}}{((p-q_2)^2-M^2+i\epsilon)((p+k-q_2)^2-M^2+i\epsilon)} \times \\
&\quad \times \frac{-i}{2p_z} v\left(\frac{\mathbf{k}^2+m_g^2+M^2x^2}{2\omega}-q_{2z}, \mathbf{q}_1\right) e^{i\frac{\mathbf{k}^2+m_g^2+M^2x^2}{2\omega}(z_1-z_0)} \tag{73}
\end{aligned}$$

In the contact limit, there are four roots which contribute to the integral over  $q_{2z}$  ( $-i\mu_2$ ,  $-i\mu_1$ ,  $\frac{\mathbf{q}_2^2}{2p_z}$  and  $(-\omega_0 - \tilde{\omega}_m)$ ), leading to

$$\begin{aligned}
M_{2,1,0}^c &= J(p+k)e^{i(p+k)x_0} a_2ca_1(T_{a_2}T_{a_1})(ig_s) \int \frac{d^2 \mathbf{q}_1}{(2\pi)^2} \frac{d^2 \mathbf{q}_2}{(2\pi)^2} e^{-i(\mathbf{q}_1+\mathbf{q}_2)\mathbf{b}_1} \times \\
&\quad \times v(0, \mathbf{q}_2)v(0, \mathbf{q}_1) \frac{(\epsilon \cdot \mathbf{k})}{\mathbf{k}^2+m_g^2+M^2x^2} e^{i\frac{\mathbf{k}^2+m_g^2+M^2x^2}{2\omega}(z_1-z_0)} \frac{1}{2i} \frac{\mathbf{k}^2+m_g^2+M^2x^2}{2\omega} \frac{\mu_1^2+\mu_1\mu_2+\mu_2^2}{\mu_1\mu_2(\mu_1+\mu_2)} \\
&\sim \frac{\omega_0}{\mu} J(p+k)e^{i(p+k)x_0} a_2ca_1(T_{a_2}T_{a_1})(ig_s) \times \\
&\quad \times \int \frac{d^2 \mathbf{q}_1}{(2\pi)^2} \frac{d^2 \mathbf{q}_2}{(2\pi)^2} e^{-i(\mathbf{q}_1+\mathbf{q}_2)\mathbf{b}_1} v(0, \mathbf{q}_2)v(0, \mathbf{q}_1) \frac{(\epsilon \cdot \mathbf{k})}{\mathbf{k}^2+m_g^2+M^2x^2} e^{i\frac{\mathbf{k}^2+m_g^2+M^2x^2}{2\omega}(z_1-z_0)} \tag{74}
\end{aligned}$$

Therefore, the contribution of  $M_{2,1,0}^c$  is suppressed by an  $O(\frac{\omega_0}{\mu})$  factor relative to the other graphs.

$$\begin{aligned}
M_{2,1,1} &= \int \frac{d^4 q_1}{(2\pi)^4} \frac{d^4 q_2}{(2\pi)^4} iJ(p+k-q_1-q_2) e^{i(p+k-q_1-q_2)x_0} \times \\
&\quad \times i\Delta_M(p+k-q_1-q_2)(-i(2p+2k-q_1-2q_2)^0)V(q_1)e^{iq_1x_1} i\Delta_M(p+k-q_2)(-i\Delta_{m_g}(k-q_2)) \times
\end{aligned}$$

$$\begin{aligned}
& \times V(q_2)e^{iq_2x_2}(-2g_s)(2E)(\epsilon \cdot (\mathbf{k} - \mathbf{q}_2))[c, a_2]a_1T_{a_2}T_{a_1} \\
= & J(p+k)e^{i(p+k)x_0}(-2ig_s)(2E)^2[c, a_2]a_1T_{a_2}T_{a_1} \times \\
& \times \int \frac{d^3\vec{\mathbf{q}}_1}{(2\pi)^3} \frac{d^3\vec{\mathbf{q}}_2}{(2\pi)^3} v(\vec{\mathbf{q}}_1)e^{-i\vec{\mathbf{q}}_1(\vec{\mathbf{x}}_1-\vec{\mathbf{x}}_0)} v(\vec{\mathbf{q}}_2)e^{-i\vec{\mathbf{q}}_2(\vec{\mathbf{x}}_2-\vec{\mathbf{x}}_0)} (\epsilon \cdot (\mathbf{k} - \mathbf{q}_2)) \times \\
& \times \Delta_M(p+k-q_1-q_2)\Delta_M(p+k-q_2)\Delta_{m_g}(k-q_2) \\
= & J(p+k)e^{i(p+k)x_0}(-2ig_s)(2E)^2[c, a_2]a_1T_{a_2}T_{a_1} \int \frac{d^2\mathbf{q}_1}{(2\pi)^2} \frac{d^2\mathbf{q}_2}{(2\pi)^2} e^{-i\mathbf{q}_1\mathbf{b}_1} e^{-i\mathbf{q}_2\mathbf{b}_2} (\epsilon \cdot (\mathbf{k} - \mathbf{q}_2)) \times \\
& \times \int \frac{dq_{2z}}{2\pi} \frac{v(\vec{\mathbf{q}}_2)e^{-iq_{2z}(z_2-z_1)}}{((k-q_2)^2 - m_g^2 + i\epsilon)((p+k-q_2)^2 - M^2 + i\epsilon)} \int \frac{dq_z}{2\pi} \frac{v(q_z - q_{2z}, \mathbf{q}_1)e^{-iq_z(z_1-z_0)}}{((p+k-q)^2 - M^2 + i\epsilon)} \\
= & J(p+k)e^{i(p+k)x_0}(-2ig_s)(2E)^2[c, a_2]a_1T_{a_2}T_{a_1} \int \frac{d^2\mathbf{q}_1}{(2\pi)^2} \frac{d^2\mathbf{q}_2}{(2\pi)^2} e^{-i\mathbf{q}_1\mathbf{b}_1} e^{-i\mathbf{q}_2\mathbf{b}_2} (\epsilon \cdot (\mathbf{k} - \mathbf{q}_2)) \times \\
& \times \int \frac{dq_{2z}}{2\pi} \frac{v(\vec{\mathbf{q}}_2)e^{-iq_{2z}(z_2-z_1)}}{((k-q_2)^2 - m_g^2 + i\epsilon)((p+k-q_2)^2 - M^2 + i\epsilon)} \times \\
& \times \frac{-i}{2p_z} v\left(\frac{\mathbf{k}^2 + m_g^2 + M^2x^2}{2\omega} - q_{2z}, \mathbf{q}_1\right) e^{i\frac{\mathbf{k}^2 + m_g^2 + M^2x^2}{2\omega}(z_1-z_0)} \tag{75}
\end{aligned}$$

In the contact limit, there are also four roots which contribute to the integral over  $q_{2z}$  ( $-i\mu_2, -i\mu_1, \frac{\mathbf{q}_2^2}{2p_z}$  and  $(\omega_2 - \omega_0)$ ). After computing the residues, we get

$$\begin{aligned}
M_{2,1,1}^c & = J(p+k)e^{i(p+k)x_0}(2ig_s)[c, a_2]a_1T_{a_2}T_{a_1} \times \\
& \times \int \frac{d^2\mathbf{q}_1}{(2\pi)^2} \frac{d^2\mathbf{q}_2}{(2\pi)^2} e^{-i(\mathbf{q}_1+\mathbf{q}_2)\mathbf{b}_1} v(0, \mathbf{q}_2)v(0, \mathbf{q}_1) \frac{(\epsilon \cdot (\mathbf{k} - \mathbf{q}_1))}{(\mathbf{k} - \mathbf{q}_1)^2 + m_g^2 + M^2x^2} \times \\
& \times e^{i\frac{\mathbf{k}^2 + M^2x^2 + m_g^2}{2\omega}(z_1-z_0)} \frac{1}{2i} \frac{(\mathbf{k} - \mathbf{q}_1)^2 + m_g^2 + M^2x^2}{2\omega} \frac{\mu_1^2 + \mu_1\mu_2 + \mu_2^2}{\mu_1\mu_2(\mu_1 + \mu_2)} \\
& \sim \frac{\omega_0}{\mu} J(p+k)e^{i(p+k)x_0}(2ig_s)[c, a_2]a_1T_{a_2}T_{a_1} \times \\
& \times \int \frac{d^2\mathbf{q}_1}{(2\pi)^2} \frac{d^2\mathbf{q}_2}{(2\pi)^2} e^{-i(\mathbf{q}_1+\mathbf{q}_2)\mathbf{b}_1} v(0, \mathbf{q}_2)v(0, \mathbf{q}_1) \frac{(\epsilon \cdot \mathbf{k})}{\mathbf{k}^2 + m_g^2 + M^2x^2} e^{i\frac{\mathbf{k}^2 + m_g^2 + M^2x^2}{2\omega}(z_1-z_0)} \tag{76}
\end{aligned}$$

We see that the contribution of  $M_{2,1,0}^c$  is also suppressed by an  $O(\frac{\omega_0}{\mu})$  factor relative to the other graphs. Therefore, we will neglect the contribution of  $M_{2,1,1}^c$  and  $M_{2,1,0}^c$  in the energy loss calculation.

## G Computation of the first order radiative energy loss

In this section we want to compute the first order in opacity radiative energy loss. According to Eq. (10) we have

$$d^3N_g^{(1)}d^3N_J = \frac{d}{dT}(\text{Tr} \langle |M_1|^2 \rangle + \frac{2}{dT} \text{ReTr} \langle M_0^* M_2 \rangle) \frac{d^3\vec{\mathbf{p}}}{(2\pi)^3 2p^0} \frac{d^3\vec{\mathbf{k}}}{(2\pi)^3 2\omega}, \tag{77}$$

$M_1$  is sum of all diagrams with one scattering center and  $M_2$  is sum of all diagrams with two scattering centers.

Using the results for  $M_{1,0,0}$ ,  $M_{1,1,0}$  and  $M_{1,0,1}$  from Appendix A we get

$$\begin{aligned}
M_1 &= M_{1,0,0} + M_{1,1,0} + M_{1,0,1} = J(p)e^{i(p+k)x_0}(-i)(2ig_s)T_{a_1} \int \frac{d^2\mathbf{q}_1}{(2\pi)^2} v(0, \mathbf{q}_1) e^{-i\mathbf{q}_1 \mathbf{b}_1} \\
&\times \left\{ \left( \frac{\epsilon \cdot (\mathbf{k} - \mathbf{q}_1)}{(\mathbf{k} - \mathbf{q}_1)^2 + m_g^2 + M^2 x^2} - \frac{\epsilon \cdot \mathbf{k}}{\mathbf{k}^2 + m_g^2 + M^2 x^2} \right) e^{i(\omega_0 + \tilde{\omega}_m)(z_1 - z_0)} [c, a_1] - \right. \\
&- \left. \frac{\epsilon \cdot (\mathbf{k} - \mathbf{q}_1)}{(\mathbf{k} - \mathbf{q}_1)^2 + m_g^2 + M^2 x^2} e^{i(\omega_0 - \omega_1)(z_1 - z_0)} [c, a_1] - \frac{\epsilon \cdot \mathbf{k}}{\mathbf{k}^2 + m_g^2 + M^2 x^2} a_1 c \right\}, \tag{78}
\end{aligned}$$

where

$$\omega_1 = \frac{(\mathbf{k} - \mathbf{q}_1)^2 + m_g^2}{2\omega}, \text{ and } \tilde{\omega}_m = \frac{M^2 x^2}{2\omega}.$$

Then,

$$\begin{aligned}
\frac{1}{d_T} \langle |M_1|^2 \rangle &= N |J(p)|^2 (4g_s^2) \frac{1}{A_\perp} \int \frac{d^2\mathbf{q}_1}{(2\pi)^2} |v(\mathbf{q}_1)|^2 \frac{C_2(T)}{d_A} \times \\
&\times \left\{ 2\alpha \left( \frac{\epsilon \cdot (\mathbf{k} - \mathbf{q}_1)}{(\mathbf{k} - \mathbf{q}_1)^2 + m_g^2 + M^2 x^2} - \frac{\epsilon \cdot \mathbf{k}}{\mathbf{k}^2 + m_g^2 + M^2 x^2} \right)^2 + 2\alpha \left( \frac{\epsilon \cdot (\mathbf{k} - \mathbf{q}_1)}{(\mathbf{k} - \mathbf{q}_1)^2 + m_g^2 + M^2 x^2} \right)^2 - \right. \\
&- 2\alpha \left( \frac{\epsilon \cdot (\mathbf{k} - \mathbf{q}_1)}{(\mathbf{k} - \mathbf{q}_1)^2 + m_g^2 + M^2 x^2} - \frac{\epsilon \cdot \mathbf{k}}{\mathbf{k}^2 + m_g^2 + M^2 x^2} \right) \frac{\epsilon \cdot (\mathbf{k} - \mathbf{q}_1)}{(\mathbf{k} - \mathbf{q}_1)^2 + m_g^2 + M^2 x^2} 2 \cos((\omega_1 + \tilde{\omega}_m)(z_1 - z_0)) - \\
&- \alpha \left( \frac{\epsilon \cdot (\mathbf{k} - \mathbf{q}_1)}{(\mathbf{k} - \mathbf{q}_1)^2 + m_g^2 + M^2 x^2} - \frac{\epsilon \cdot \mathbf{k}}{\mathbf{k}^2 + m_g^2 + M^2 x^2} \right) \frac{\epsilon \cdot \mathbf{k}}{\mathbf{k}^2 + m_g^2 + M^2 x^2} 2 \cos((\omega_0 + \tilde{\omega}_m)(z_1 - z_0)) + \\
&+ \alpha \frac{\epsilon \cdot \mathbf{k}}{\mathbf{k}^2 + m_g^2 + M^2 x^2} \frac{\epsilon \cdot (\mathbf{k} - \mathbf{q}_1)}{(\mathbf{k} - \mathbf{q}_1)^2 + m_g^2 + M^2 x^2} 2 \cos((\omega_0 - \omega_1)(z_1 - z_0)) + \\
&+ \left. \left( \frac{\epsilon \cdot \mathbf{k}}{\mathbf{k}^2 + m_g^2 + M^2 x^2} \right)^2 \text{Tr} a^2 c^2 \right\} \tag{79}
\end{aligned}$$

Here we used  $\text{Tr}(T_{a_1} T_{a_2}) = \frac{C_2(T) d_T}{d_A} \delta_{a_1 a_2}$ , and defined  $\alpha \equiv \text{Tr}(c^2 a^2 - c a c a)$ . Factor  $N$  comes from sum over  $N$  scattering centers.

To compute  $M_2$  we will first add all the diagrams with two scattering centers calculated in Appendix B-E, and then take their average.

$$\begin{aligned}
M_2 &= \frac{1}{2} J(p) e^{i(p+k)x_0} (-2ig_s) T_{a_1} T_{a_2} \frac{1}{A_\perp} \int \frac{d^2\mathbf{q}_1}{(2\pi)^2} |v(\mathbf{q}_1)|^2 \\
&\times \left\{ \frac{\epsilon \cdot \mathbf{k}}{\mathbf{k}^2 + m_g^2 + M^2 x^2} \left\{ e^{i(\omega_0 + \tilde{\omega}_m)(z_1 - z_0)} ([c, a_2], a_1] + [a_2 a_1, c]) - [[c, a_2], a_1] - a_2 a_1 c \right\} - \right. \\
&- \left. \frac{\epsilon \cdot (\mathbf{k} - \mathbf{q}_1)}{(\mathbf{k} - \mathbf{q}_1)^2 + m_g^2 + M^2 x^2} \left( e^{i(\omega_0 + \tilde{\omega}_m)(z_1 - z_0)} - e^{i(\omega_0 - \omega_1)(z_1 - z_0)} \right) (a_2 [c, a_1] + a_1 [c, a_2]) \right\} \tag{80}
\end{aligned}$$

Using this we can now find  $\frac{2}{d_T} \text{ReTr} \langle M_0^* M_2 \rangle$ .

$$\begin{aligned}
\frac{2}{d_T} \text{ReTr} \langle M_0^* M_2 \rangle &= N |J(p)|^2 (4g_s^2) \frac{1}{A_\perp} \int \frac{d^2 \mathbf{q}_1}{(2\pi)^2} |v(\mathbf{q}_1)|^2 \frac{C_2(T)}{d_A} \\
&\times \left\{ \left( \frac{\boldsymbol{\epsilon} \cdot \mathbf{k}}{\mathbf{k}^2 + m_g^2 + M^2 x^2} \right)^2 (2\alpha \cos((\omega_0 + \omega')(z_1 - z_0)) - 2\alpha - \text{Tra}^2 c^2) + \right. \\
&+ 2\alpha \frac{\boldsymbol{\epsilon} \cdot \mathbf{k}}{\mathbf{k}^2 + m_g^2 + M^2 x^2} \frac{(\boldsymbol{\epsilon} \cdot (\mathbf{k} - \mathbf{q}_1))}{(\mathbf{k} - \mathbf{q}_1)^2 + m_g^2 + M^2 x^2} \\
&\left. \times \{ \cos((\omega_0 + \tilde{\omega}_m)(z_1 - z_0)) - \cos((\omega_0 - \omega_1)(z_1 - z_0)) \} \right\} \quad (81)
\end{aligned}$$

Therefore,  $\frac{1}{d_T} \langle |M_1|^2 \rangle + \frac{2}{d_T} \text{ReTr} \langle M_0^* M_2 \rangle$  is equal to

$$\begin{aligned}
\frac{1}{d_T} \langle |M_1|^2 \rangle + \frac{2}{d_T} \text{ReTr} \langle M_0^* M_2 \rangle &= D_R |J(p)|^2 (4g_s^2) \frac{C_2(T)}{d_A} C_R^2 \frac{1}{A_\perp} \int \frac{d^2 \mathbf{q}_1}{(2\pi)^2} |v(\mathbf{q}_1)|^2 \\
&\times \left\{ -2 \frac{(\boldsymbol{\epsilon} \cdot (\mathbf{k} - \mathbf{q}_1))}{(\mathbf{k} - \mathbf{q}_1)^2 + m_g^2 + M^2 x^2} \left( \frac{\boldsymbol{\epsilon} \cdot \mathbf{k}}{\mathbf{k}^2 + m_g^2 + M^2 x^2} - \frac{(\boldsymbol{\epsilon} \cdot (\mathbf{k} - \mathbf{q}_1))}{(\mathbf{k} - \mathbf{q}_1)^2 + m_g^2 + M^2 x^2} \right) \times \right. \\
&\left. \times \left( 1 - \cos\left( \frac{(\mathbf{k} - \mathbf{q}_1)^2 + m_g^2 + M^2 x^2}{2p_z x} (z_1 - z_0) \right) \right) \right\}. \quad (82)
\end{aligned}$$

Here we have used that  $\omega_1 + \tilde{\omega}_m = \frac{(\mathbf{k} - \mathbf{q}_1)^2 + m_g^2 + M^2 x^2}{2p_z x}$  and  $\alpha = \frac{1}{2} C_R^2 D_R$ .

Using Eqs. (10, 8) it is now easy to extract  $dE_{ind}^{(1)} \equiv \omega d^3 N_g$

$$\begin{aligned}
\frac{dE_{ind}^{(1)}}{dx} &= \frac{C_R \alpha_S L}{\pi \lambda} E \int \frac{d^2 \mathbf{q}_1}{\pi} \frac{\mu^2}{(\mathbf{q}_1^2 + \mu^2)^2} \int \frac{d^2 \mathbf{k}}{\pi} \times \\
&\times \left\{ -2 \frac{(\boldsymbol{\epsilon} \cdot (\mathbf{k} - \mathbf{q}_1))}{(\mathbf{k} - \mathbf{q}_1)^2 + m_g^2 + M^2 x^2} \left( \frac{\boldsymbol{\epsilon} \cdot \mathbf{k}}{\mathbf{k}^2 + m_g^2 + M^2 x^2} - \frac{(\boldsymbol{\epsilon} \cdot (\mathbf{k} - \mathbf{q}_1))}{(\mathbf{k} - \mathbf{q}_1)^2 + m_g^2 + M^2 x^2} \right) \times \right. \\
&\left. \times \int dz_1 \left( 1 - \cos\left( \frac{(\mathbf{k} - \mathbf{q}_1)^2 + m_g^2 + M^2 x^2}{2p_z x} (z_1 - z_0) \right) \right) \right\} \frac{e^{-\frac{(z_1 - z_0)}{L}}}{L}, \quad (83)
\end{aligned}$$

where we have used Eqs. (1, 6) from [16] to write the result in terms of opacity  $L/\lambda$ . For simplicity we have also assumed exponential distribution  $\exp(-\Delta z/L)/L$  between scattering centers. After the  $z_1$  integration we get

$$\begin{aligned}
\frac{dE_{ind}^{(1)}}{dx} &= \frac{C_R \alpha_S L}{\pi \lambda} E \int \frac{d\mathbf{k}^2}{\mathbf{k}^2 + m_g^2 + M^2 x^2} \int \frac{d^2 \mathbf{q}_1}{\pi} \frac{\mu^2}{(\mathbf{q}_1^2 + \mu^2)^2} \times \\
&\times 2 \frac{\mathbf{k} \cdot \mathbf{q}_1 (\mathbf{k} - \mathbf{q}_1)^2 + (m_g^2 + M^2 x^2) \mathbf{q}_1 \cdot (\mathbf{q}_1 - \mathbf{k})}{\left( \frac{4Ex}{L} \right)^2 + ((\mathbf{k} - \mathbf{q}_1)^2 + M^2 x^2 + m_g^2)^2} \quad (84)
\end{aligned}$$

which in the massless limit reduces to Eq (125) from [16].

## References

- [1] S. S. Adler *et al.* [PHENIX Collaboration], Phys. Rev. Lett. **91**, 072301 (2003) [arXiv:nucl-ex/0304022].
- [2] K. Adcox *et al.* [PHENIX Collaboration], Phys. Lett. B **561**, 82 (2003) [arXiv:nucl-ex/0207009].
- [3] K. Adcox *et al.* [PHENIX Collaboration], Phys. Rev. Lett. **88**, 022301 (2002) [arXiv:nucl-ex/0109003].
- [4] J. Adams *et al.* [STAR Collaboration], arXiv:nucl-ex/0305015.
- [5] C. Adler *et al.* [STAR Collaboration], Phys. Rev. Lett. **90**, 082302 (2003) [arXiv:nucl-ex/0210033].
- [6] C. Adler *et al.* [STAR Collaboration], Phys. Rev. Lett. **90**, 032301 (2003).
- [7] C. Adler *et al.*, [STAR Collaboration] Phys. Rev. Lett. **89**, 202301 (2002) [arXiv:nucl-ex/0206011].
- [8] Proc. 15th Int. Ultra. Nucleus-Nucleus Coll. (Quark Matter 2001, Jan. SUNY), Nucl.Phys. A **698** (2002) 1c; Proc. 16th (Quark Matter 2002, July Nantes, France); Nucl. Phys. A715 (2003) 1c.
- [9] M. Gyulassy, P. Levai, and I. Vitev, Phys. Lett. B **538**, 282 (2002) ; E. Wang and X.-N. Wang, Phys. Rev. Lett. **89**, 162301 (2002); C. A. Salgado and U. A. Wiedemann, Phys. Rev. Lett. **89**, 092303 (2002); M. Gyulassy, I. Vitev and X. N. Wang, Phys. Rev. Lett. **86**, 2537 (2001).
- [10] M. Gyulassy, I. Vitev, X. N. Wang and B. W. Zhang, arXiv:nucl-th/0302077.
- [11] X. N. Wang, Phys. Rev. C **61**, 064910 (2000) [arXiv:nucl-th/9812021]; X. N. Wang, Phys. Lett. B **565**, 116 (2003) [arXiv:nucl-th/0303004].
- [12] I. Vitev and M. Gyulassy, Phys. Rev. Lett. **89**, 252301 (2002) [arXiv:hep-ph/0209161]. I. Vitev, Phys. Lett. B **562**, 36 (2003) [arXiv:nucl-th/0302002]. A. Accardi and M. Gyulassy, arXiv:nucl-th/0308029.
- [13] R. Baier, D. Schiff, B. G. Zakharov, Ann. Rev. Nucl. Par. Sci. **50** 37 (2000). B.G. Zhakharov, JETP Lett. **63**, 952 (1996); R. Baier *et al.*, Nucl. Phys. B **484**, 265 (1997); R. Baier, Yu. L. Dokshitzer, A. H. Mueller, D. Schiff, Phys. Rev. C **58** 1706 (1998);
- [14] U.A. Wiedemann, Nucl. Phys. B **588**, 303 (2000), Nucl. Phys. B **582** 409 (2000).
- [15] M. Gyulassy, P. Levai, and I. Vitev, Phys. Rev. Lett. **85**, 5535 (2000) ; Phys. Rev. D **66**, 014005 (2002).
- [16] M. Gyulassy, P. Levai, and I. Vitev, Nucl. Phys. B **594**, 371 (2001).
- [17] M. Gyulassy, X. N. Wang, Nucl. Phys. B **420** 583 (1994);
- [18] X. N. Wang, M. Gyulassy, M. Plumer, Phys. Rev. D **51** 3436 (1995).
- [19] X. N. Wang, Phys. Rev. Lett. **81** 2655 (1998); Phys. Rev. C **58** 2321 (1998).
- [20] M. Gyulassy and M. Plumer, Nucl. Phys. A **527**, 641 (1991). M. Gyulassy, M. Plumer, M. Thoma and X. N. Wang, Nucl. Phys. A **538**, 37C (1992) ; X. Wang and M. Gyulassy, Phys. Rev. Lett. **68**, 1480 (1992).
- [21] J. D. Bjorken, FERMILAB-PUB-82-059-THY and erratum (unpublished); M. H. Thoma and M. Gyulassy, Nucl. Phys. B **351**, 491 (1991); E. Braaten and M. H. Thoma, Phys. Rev. D **44**, 2625 (1991); M. H. Thoma, J. Phys. G **26**, 1507 (2000) [arXiv:hep-ph/0003016].
- [22] S. S. Adler *et al.* [PHENIX Collaboration], Phys. Rev. Lett. **91**, 072303 (2003) [arXiv:nucl-ex/0306021].
- [23] J. Adams *et al.* [STAR Collaboration], Phys. Rev. Lett. **91**, 072304 (2003) [arXiv:nucl-ex/0306024].

- [24] I. Arsene *et al.* [BRAHMS Collaboration], suppression,” Phys. Rev. Lett. **91**, 072305 (2003) [arXiv:nucl-ex/0307003].
- [25] B. B. Back *et al.* [PHOBOS Collaboration], Phys. Rev. Lett. **91**, 072302 (2003) [arXiv:nucl-ex/0306025].
- [26] E. V. Shuryak, Phys. Rev. C **55**, 961 (1997)
- [27] M. G. Mustafa, D. Pal, D. K. Srivastava and M. Thoma, Phys. Lett. B **428**, 234 (1998)
- [28] Z. W. Lin and R. Vogt, Nucl. Phys. B **544**, 339 (1999) Z. W. Lin, R. Vogt and X. N. Wang, Phys. Rev. C **57**, 899 (1998)
- [29] Y. L. Dokshitzer and D. E. Kharzeev, Phys. Lett. B **519**, 199 (2001)
- [30] K. Adcox *et al.* [PHENIX Collaboration], Phys. Rev. Lett. **88**, 192303 (2002).
- [31] S. Batsouli, S. Kelly, M. Gyulassy, J. L. Nagle, Phys. Lett. B **557**, 26 (2003).
- [32] M. Djordjevic and M. Gyulassy, Phys. Lett. B **560**, 37 (2003) [arXiv:nucl-th/0302069].
- [33] M. Djordjevic and M. Gyulassy, Phys. Rev. C **68**, 034914 (2003) [arXiv:nucl-th/0305062].
- [34] B. W. Zhang, E. Wang and X. N. Wang, arXiv:nucl-th/0309040.
- [35] J. F. Gunion, G. Bertsch, Phys. Rev. D **25**, 746 (1982).
- [36] Levai P, Papp G, Fai G, Gyulassy M, Barnafoldi G G, Vitev I, Zhang Y, Nucl. Phys. A **698** 631 (2002).
- [37] M. Gyulassy, P.Levai, I. Vitev, Nucl. Phys. B **571**, 197 (2000).
- [38] M. Gyulassy, P.Levai, I. Vitev, Nucl. Phys. B **661**, 637c (1999).
- [39] A. Adil, M. Gyulassy, I. Vitev, in preparation.